Department of Mechanical Engineering
2019-02-06 | Version 1.1

Displacement fluid mechanics in primary cemented annuli

Final Report for BCOGRIS project EI-2016-10

Ian A. Frigaard & Amir Maleki

Parts of this research have been conducted using funding from the following organizations, to whom we express our sincere appreciation:

BC OGRIS
BC Oil and Gas Research and Innovation Society
NSERC CRSNG
Schlumberger
SINTEF
The Research Council of Norway

UBC THE UNIVERSITY OF BRITISH COLUMBIA

Table of Content

Executive Summary

This is a final report for work on the project “Displacement fluid mechanics in primary cemented annuli”, which has been conducted at the University of British Columbia, Department of Mechanical Engineering, primarily by Dr. Amir Maleki under the supervision of Prof. Ian Frigaard. This work forms the main part of the PhD thesis of Dr. Maleki (Sept 2014- Nov 2018), as well as the MASc thesis of Ms. Nikoo Hanachi (May 2016-May 2018). A number of published papers describing project results are listed at the end of this report. Both theses are publicly available permanent records of the research, available at: http://hdl.handle.net/2429/67903 and99 http://hdl.handle.net/2429/65133.

This work has been funded primarily by the British Columbia Oil & Gas Commission (BCOGC) through BC Oil and Gas Research and Innovation Society (BC OGRIS) (project number EI-2016-10). Earlier work on this project was initiated under a larger collaborative research and development grant between Schlumberger and NSERC (CRD project number 444985-12: “Topics in Oilfield Cementing Fluid Mechanics”). There was some overlap in the scope and duration of these projects and we also extended the scope into areas such as foamed cementing. Later in the project an additional collaboration was established with SINTEF Industries through project number 268510 of the Norwegian Research Council, which offered exciting opportunities for extending the application range of our model. We acknowledge the above funding sources with gratitude. We would also like to express our appreciation to J. Nurokowski (BCOGC) and J. Kitchen (BCOGC, now at ARC Resources) for actively following the research projects.

It is widely agreed upon that roughly about 10-20% of wells in western Canada leak to various degrees (Dusterhoft et al, 2002; Dusseault et al, 2014; Atherton et al, 2017). Similar rates are reported worldwide. The concerns are various, depending on the stakeholder: reduced productivity (due to reservoir pressure reduction), environmental (emissions and damage to near-surface ecology), health (groundwater pollution or emitted gas toxicity), public perception, regulatory effectiveness. There are many reasons why and how the integrity of a cemented well is compromised. A good number of these reasons stem from fluid mechanics of initial displacement. The main difficulty of the displacement arises from three factors:

- **Geometry:** the annular region is only 2-3 cm wide on average and extends 100-1000 m along the well in a typical cemented stage. In addition, even in nominally vertical annuli, it is common that the annulus is eccentric which induces an unfavorable flow bias.
- **Rheology:** drilling muds are yield stress materials, meaning that they have the tendency to become stuck on the narrow side of the annulus, as well as on the walls and potentially filling vuggy wellbore irregularities.
- **Fluid Mechanics:** in addition to drilling muds, spacers and cement slurries are shear-thinning yield stress materials. Understanding flows of these fluids with significant buoyancy forces and rheological differences in long narrow annuli is far from classical fluid mechanics and requires specialized knowledge and attention.

From an operational perspective fluid mechanics enters into the design in 3 ways. (i) What are the properties of the fluids that we pump: density and rheology (which relates to the structure and viscosity of the fluid)? (ii) How much of

each fluid should be pumped? (iii) How fast should the fluids be pumped? For each question there are both constraints and flexibility (e.g. adjusting cement rheology via additives). A combination of (i) and (iii) determines whether the well is cemented in turbulent or laminar flow. Depending on local geometry and fluid properties as well as the overall imposed flow rate, it is relatively common within the annulus that one fluid can be fully turbulent (e.g. a chemical wash or low-viscous spacer) while others are laminar. Indeed, this can also happen in a single fluid around the annulus, where the flow is turbulent on the wide side and laminar (or even stuck) on the narrow side.

Although turbulent and mixed flow regimes commonly occur in primary cementing operations, there is no study in the literature that systematically analyzes these flows and quantitatively compare them with laminar flows. The aim of the present project is to fill this gap in knowledge. While the focus is on turbulent flows, the derivation of our new model is consistent with (and incorporates) previous laminar models, which allows us to effectively simulate mixed flow regimes.

Having established a framework to study turbulent and mixed flow regime displacement flows, we are able to analyze a broad range of industrial practices and reassess if the supposed outcomes are consistent with the physical and scientific reasoning embodied in the model. This is particularly important in primary cementing where downhole measurement is difficult, there is little systematic evaluation of success and poor industrial record keeping of design aspects. A brief summary of the projects is presented below. More details of these projects can be found later in the report. Based on the results we have made a number of best practices recommendations.

Project 1: Estimate of mixing in turbulent displacement flows

Project 1 gives a leading order estimate for the mixing in turbulent displacement flows in annular geometries. This project is of major significance, because mixing is the chief factor that differentiates laminar and turbulent displacement flows. In laminar displacement flows, the only mechanism for mixing is governed by molecular diffusion. A simple scaling analysis proves that within the time-scale of cementing, molecular diffusion does not play any significant role. However, in turbulent displacement fluids, in addition to molecular diffusion, mixing is enhanced by turbulent diffusion. Turbulent diffusion is several orders of magnitude larger than molecular diffusion, and therefore plays a more important role in the displacement outcome. More importantly, turbulent displacement flows fall into a Taylor dispersion regime. Our analysis showed that the effect of Taylor dispersion is one or two orders of magnitude larger than turbulent diffusion. This effectively means any turbulent model should account for the effects of Taylor dispersion.

In order to estimate Taylor dispersion and turbulent diffusion, an accurate profile of turbulent velocity is necessary. The well-known log-law turbulent velocity profile has two deficiencies: it does not satisfy the no slip condition at the wall and the symmetry condition at the centreline. In Maleki and Frigaard (2016) we laid down a consistent framework for hydraulic calculations for shear-thinning yield stress fluids. This framework was then employed to obtain a more complete turbulent velocity profile. Our framework was adopted from the phenomenological approach of Metzner-Reed (Metzner and Reed, 1955; Dodge and Metzner, 1959). We particularly show that in the limit of weakly turbulent flows, the velocity correction near the wall significantly influences our estimate of Taylor dispersion. In addition, the

Taylor diffusivity is two or more orders of magnitude larger than the turbulent diffusion coefficient. In addition, we analyzed the role of rheological parameters, namely the shear-thinning index (n) as well as the yield stress (τ_Y) on transition to turbulence. We showed that as the fluid become more shear-thinning or the yield stress increases, transition to turbulent is delayed and the mixing mechanisms (both diffusion and dispersion) are supressed.

Project 2: Multi-regime annular displacement model

Project 2 is core of our work. Here, our goal was to derive a 2D model for the displacement of shear-thinning yield stress fluids in eccentric annular geometries. The model is based on the assumption that the annular gap is narrow. This allows to average the radial variations and reduce the problem into 2D. To the leading-order, the narrow gap approximation simplifies the momentum equations to a turbulent shear flow in the direction of the modified pressure gradient. This is the natural extension of the laminar displacement model in Bittleston et al. (2002). The mass transport equations are however quite different than those in the laminar model, because of the effects of turbulent diffusion and Taylor dispersion. Changes in concentrations within the annular gap arise due to the combined effects of advection with the mean flow, anisotropic Taylor dispersion (along the streamlines) and isotropic turbulent diffusivity. The diffusive and dispersive effects are modelled for fully turbulent and transitional flows in Project 1.

While the focus of the derivation was to model turbulent displacement flows, the model is derived in a general framework that allows to include laminar and mix flow regimes as well. More specifically, the model includes a nonlinear elliptic equation for the streamfunction. This equation is similar to those commonly found in flows in porous media or Hele-Shaw cells. We have performed additional theoretical analysis that confirms existence and uniqueness of the solution. Upon solving this equation, a velocity field can be readily calculated by differentiating the streamfunction. This velocity field is then inserted into an advection-diffusion equation that governs concentration of each fluid in the annulus; see Maleki and Frigaard (2017) for more details.

We subsequently studied a number of case studies, investigating the role of density difference, viscosity difference and geometrical parameters in turbulent and mixed flow regime. We have also investigated the effect of flow regime on the displacement outcome. Notably, and quite on the contrary to many industrial guideline, we did not identify any significant difference between comparable displacement case studies run in laminar and turbulent regimes.

Project 3: A model for foamed cementing

In project 3, we focused on modelling displacement flows involving foamed cements. Foamed cements are weakly compressible materials which consist of a base cement slurry that suspends a gas phase, typically nitrogen. Foamed cements have low density and exhibit higher ductility and higher tensile strength when dehydrate, compared to their conventional counterparts. Some studies show better zonal isolation in foamed cement wells, particularly in wells with high temperature and pressure.

In project 3, we first have derived a simple 1D hydraulics-based model for the displacement flow. We have also simplified this model to a purely hydrostatic model and used the comparison between the two models to show that in many cases the frictional pressure losses can be neglected relative to the hydrostatic pressure. Because these types of models are only in 1D, they are inherently incapable of capturing density-driven instabilities that might grow as a result of expansion of foamed cement. Therefore, in the main part of the project 3, we aimed to extend the narrow-gap annular displacement model of Bittleston et al (2002) to allow compressibility. We accomplished this goal by working with mass streamfunction instead of volumetric streamfunction.

Project 4: Interface tracking in primary cementing

Project 4 was carried out in collaboration with SINTEF Industries and is funded by the Research Council of Norway. The objective of project 4 is to design new ways to obtain more accurate and reliable quality control of primary cementing operations. The motivation for better evaluation of cement placement here is to allow the use of depleted reservoirs for purposes such as Carbon Capture and Storage (CCS), in which case the well is a conduit that penetrates the caprock and thus must be sealed/controlled.

Currently, the quality of a cement job is evaluated using a variety of logging models such as cement bond log (CBL), variable density log (VDL), UltraSonic Imager Tool (USIT), etc. The most common is CBL which measures acoustic amplitude, travel time, and attenuation. Interpretation of the signals infers information about how well the cement is bonded to the inside of the casing. CBL generally involves a costly time delay, and therefore, it is not run on the majority of cement jobs, directly afterwards. In addition, since logging is performed after the cement is set, no corrective measures can be pursued if the cement job has gone badly wrong, except performing remedial cementing later, which is expensive and not always effective.

In project 4, a new methodology for tracking the interface of annular displacement flows has been proposed and evaluated. The method is based on exploiting the density difference between successive fluids pumped in order to design a tracer particle to sit at the interface. Although apparently trivial, such particles must overcome viscous drag and strong secondary flows in order to reach and remain at the interface. Successful tracking of the interface allows to detect displacement and geometric anomalies in real time, instantaneously determine the top of cement and monitor post-placement fluid motions.

Our 1D and 2D computational analyses confirm that for some ranges of parameters relevant to laminar primary cementing, the method presented here is feasible for vertical annuli (i.e. the particles reach to the interface, regardless of their release position and velocity, and remain stuck to the interface). As the density difference shrinks and the carrier fluid becomes more viscous, it takes longer distance for the particles to reach to the interface. Eventually, at some combination of density difference and (effective) viscosity, the particles instead attain a secondary equilibrium state, which is far from the interface. This is where the methodology fails. The experimental phase of project 4 is currently carried out at the SINTEF facilities in Trondheim, Norway.

Best Practices Recommendations

1. Our analysis repeatedly confirms that the single most critical parameter in primary cementing flows is eccentricity. This has been known since the 1960s, but various factors conspire against effective centralization, e.g. drillers and operators do not understand the importance and continually advocate for less centralizers in favour of reducing risks of the casing becoming stuck on being placed. There is also a common perception that a vertical section will be centralized which is discredited according to several case studies (e.g. see Guillot et al (2008); Gorokhova et al (2014)). We find the API recommendation for eccentricity ($e \leq 0.33$) a reliable guideline in that with such eccentricities we are usually able to ensure an effective displacement using a combination of density differences and either turbulent flow or laminar flow with rheology. However, with such eccentricities it is still necessary to work hard on the fluids and flows, i.e. $e \leq 0.33$ is a necessary condition only.

   We strongly advocate for rigorous implementation of centralizing strategies, consistent recording of designs implemented and some form of post-placement evaluation.

2. The next parameter that plays a crucial role in primary cementing flows is density difference. In a vertical well, it is absolutely necessary for the displacing fluid to be heavier than the displaced fluid. This buoyancy force competes against the effects of eccentricity and make the displacement to progress more steadily. In addition, the buoyancy forces mobilize the mud on the narrow side, which eliminates or reduce formation of mud layers. The industrial guidelines typically prescribe a 10% density difference to be sufficient. However, our simulations disagree with this general statement. The necessary density difference depends on the rheology of the fluid, especially the yield stress, as well as the eccentricity of the well, and sometimes a density difference as large as 20% may be necessary to ensure a steady displacement. In more extreme cases, when the annulus is highly eccentric ($e \geq 0.6$) and mud has a large yield stress ($\tau_Y \geq 10$ Pa), the displacement remains unsteady even at the presence of >50% density difference.

3. There is a widely accepted perception in the cementing community that turbulent displacement is necessarily superior to laminar displacement. However, our simulations show no clear indication that turbulent displacement always outperforms laminar displacement. In fact, we have shown examples where a highly viscous preflush in a lower Reynolds number displacement flow outperformed the fully turbulent, and vice versa. Many mixed regime displacement flows were also studied and found to be of similar effectiveness. Instead of prescribing the displacement regime, we recommend the operators to ensure the well is sufficiently centralized, and enough density difference is accounted for.

4. We showed that in fully turbulent displacement flows, the fluids rheological parameters lose their importance. This effectively means the only mechanism to control turbulent flows is buoyancy. Recall that in laminar flows,

the displacement can be controlled by both the buoyancy forces and rheological differences. This suggests that turbulent displacement flows are more difficult to control.

5. When the displacement regime is fully turbulent, increasing flow rate may lead to loss of steady displacement. This is because at larger flow rates the turbulent stresses entirely dominate the buoyancy stresses. Consequently, the displacement becomes unsteady. A common implication of this rule is in the application of low-weight washes. (Increasing flow rate of washes does not improve their displacement performance).

6. Volumetric displacement efficiency is a common way to measure quality of the displacement outcome. However, because of the eccentricity of annuli, high values of efficiency (>90%) can be achieved, even when the narrow side is not cemented at all. In selecting a measure of success, the volumetric bias in the displacement efficiency needs to be countered. We proposed to use mix of various efficiency measurement including our narrow side efficiency.

7. The notion that light-weight low-viscous washes can provide cleaning is generally flawed. When using washes, the wash progressively advances ahead of the lead slurry, channeling rapidly up the wide side of the annulus. Even when fully turbulent, it is ineffective at displacing mud from around the annulus. In addition, washes do not provide any form of barrier between slurry and mud. We generally advocate for using preflushes that are sufficiently heavier and more viscous than the mud.

8. Contact time is a poor measure of chemical cleaning. Our simulations show the distribution of contact time in the annulus is highly non-uniform. This means while the nominal necessary contact time is met, large areas of the annulus have not been in contact with the fluid. Even worse, increasing the nominal contact time does not improve necessarily help with the contact time. Instead of such bulk simplistic measurements, we advocate for local measurement through numerical simulations, such as those presented in this project.

9. In terms of regulatory requirements, our first recommendation is simple. BCOGC collects a large amount of well data in its database, deposited there by operators. A glaring hole in the data gathered is that concerning cementing. The fact that the data is not collected systematically prevents many standard forms of process improvement, e.g. even determining what current practice is by means of an elementary statistics. If the effectiveness of cementing is to be improved, the following minimal data should be stored for each cementing operation

    a. Information regarding centraliser deployment, i.e. number fitted and where, type etc

    b. Any further geometric information regarding the hole size, e.g. caliper runs

    c. Fluid densities

d. Fluid viscosities, i.e. of every fluid in the well (mud, preflushes, cement slurries). Readings from a standard 6 (or 12) speed oilfield viscometer should be made and stored at rigsite.

e. Flowrates/pump schedule and fluid volumes pumped, (actual), plus any observations from the job, e.g. time when the cement is seen at surface

f. Commercial names of the blends pumped for any slurry, spacer etc

10. The second area where we recommend regulatory improvement is in evaluation of the effectiveness of the primary cementing job. At present the only standard information available is simply from a pressure test and from records of returns to surface. The problem with this is there is no feedback on individual mechanisms of failure and hence no help to remedy those parts of the process that might be identified as defective.

    For example, if SCVF is later detected in a well, but at low rate, the operator may decide to defer repair until abandonment under the current regulations. Since this is typically 10+ years later, there is no opportunity to learn directly from the information from e.g. CBL, and improve the actual cementing. Especially in BC, where we are often pad drilling, learning from the previous well is of clear value. For example, depending on the logging tool it is possible to infer positioning of centralisers and also to make comparisons between CBL output and information from displacement simulations: fluid maps, etc. This type of evaluation criteria and fluid map comparison appears in many recent SPE papers with cementing case studies.

    The issue is that measures such as requiring a CBL (or similar test) to be run after each test represent a cost increase on the price of completing the well. The benefits however to the industry in terms of better process designs, technical advances, better productivity and cheaper eventual abandonment costs probably outweigh the cost.

Tangible outcomes

Apart from the best practices recommendations, the main contributions are in published studies and in software.

Published studies

Having developed a model and our own physical intuition regarding turbulent displacement flows, we have then systematically addressed different common practices that relate to turbulent flows. Published work is listed at the end of this report. The 4 key features that our work has highlighted are:

1. In a fully turbulent flow, pumping too fast is likely to result in a poor displacement, perhaps contrary to expectations.

2. Classifying a displacement as laminar or turbulent hides the fact that many cementing flows have multiple regimes. These mixed regimes do not have "design rules" in place.

3. Using lightweight non-viscous preflushes (washes) is likely to be ineffective.

4. There is no conclusive evidence that a laminar or turbulent displacement is universally better when a realistic comparison is made. By realistic we mean within the constraints of the process on any given well.

The above features are partly dependent on the model developed, but not too much on the specifics, e.g. using a slightly different frictional pressure closure. Thus, we believe that these are robust conclusions, each documented in a careful study. This is an area where there has been essentially no analysis of the fluid mechanics of turbulent cementing displacements. At the very least, we feel that industrial cementers should take note that all is not as was believed and take steps to correct their intuition.

Software Package OGRE

The second tangible outcome of this project is the development of a software package (OGRE) that encapsulates the model derived in this project. The package is developed in MATLAB for the purpose of ease of maintainability and portability. The code utilizes a variant of the augmented Lagrangian method to fully resolve the viscoplastic fluids. Furthermore, several features, including geometric variations, pumping schedule as well as various rheological inputs are available. For the purpose of accessibility, a basic GUI is designed in MATLAB that allows any user with no specific knowledge of the underlying algorithms to interact with the package and simulate various displacement scenarios.

At present the software has been developed for research use, but could be adapted and developed in a way suitable for industry and the regulator to use.

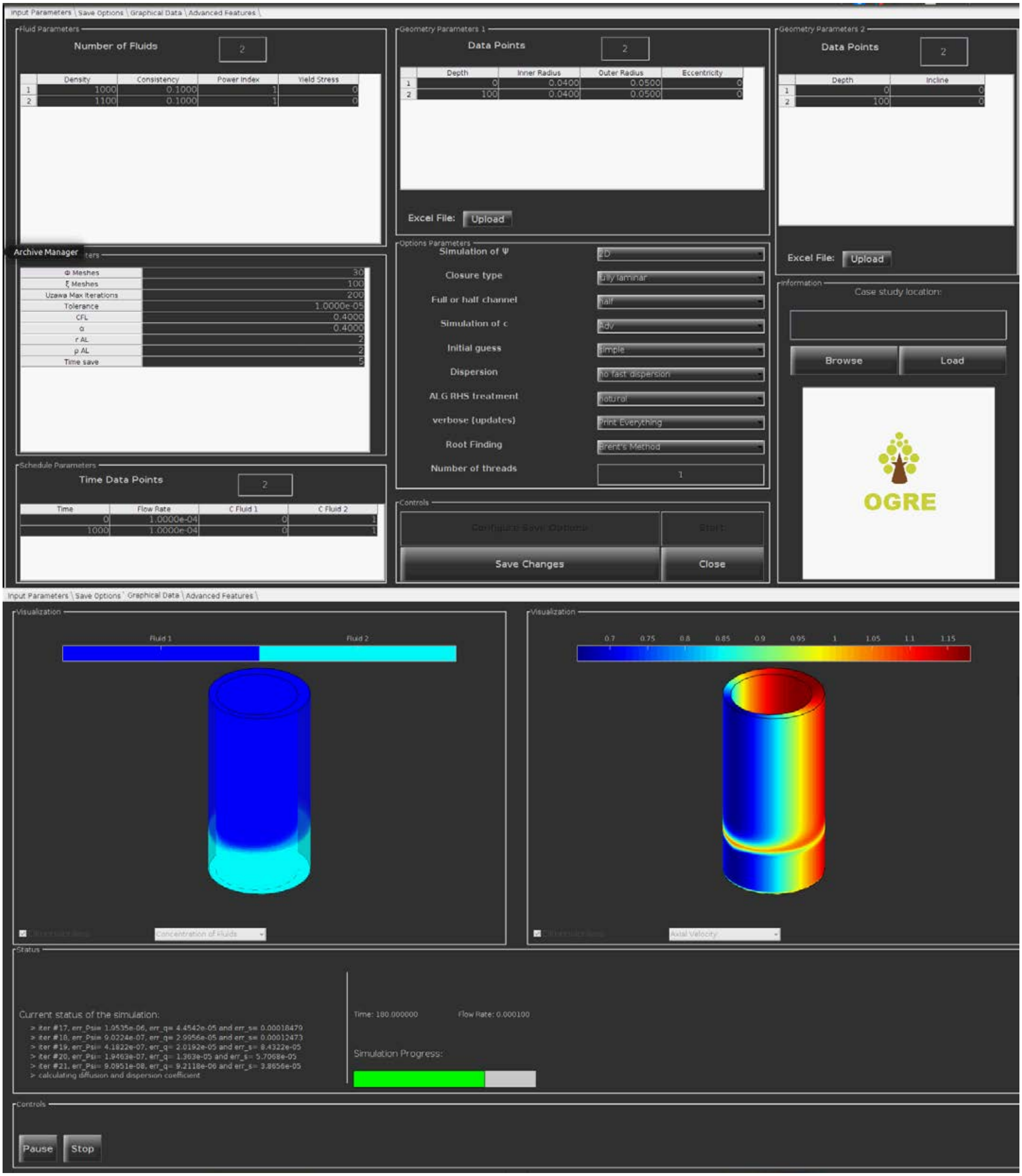

Graphic User Interface for the OGRE package

Background

The primary cementing process proceeds as follows; see Fig. 1. A new section of the well is drilled. The drillpipe is removed from the wellbore, leaving drilling mud inside the wellbore. A steel tube (casing or liner) is inserted into the wellbore, typically leaving a mean annular gap of ≈ 2-3 cm. The tubing is inserted in sections of length ≈ 10 m each, threaded together so that cemented sections can extend 100–1000 m. So-called centralizers are fitted to the outside of the tube, to prevent the heavy steel tubing from slumping to the lower side of the wellbore. However, even in (nominally) vertical wells it is common that the annulus is eccentric and this is especially true in inclined and horizontal wells. With the steel casing in place and drilling mud on the inside and outside, the operation begins. First, the drilling mud is conditioned by circulating around the flow path. Next a sequence of fluids is circulated down the inside of the casing and returning up the outside of the annulus. Preflushes (washes or spacer fluids) are followed by one or more cement slurries. The fluid volumes are designed so that the cement slurries fill the annular space to be cemented. Drilling mud follows the final cement slurry to be pumped and the operations end with the cement slurry held in the annulus (with a valve system) and allowed to hydrate (i.e. set) over a period of many hours. With reference to Fig. 1, it can be seen that the completed well often has a telescopic arrangement of casings and liners. Thus, the operation is repeated more than once on most wells. Typically, inner diameters can start at anything up to 50 cm and can end as small as 10 cm in the producing zone.

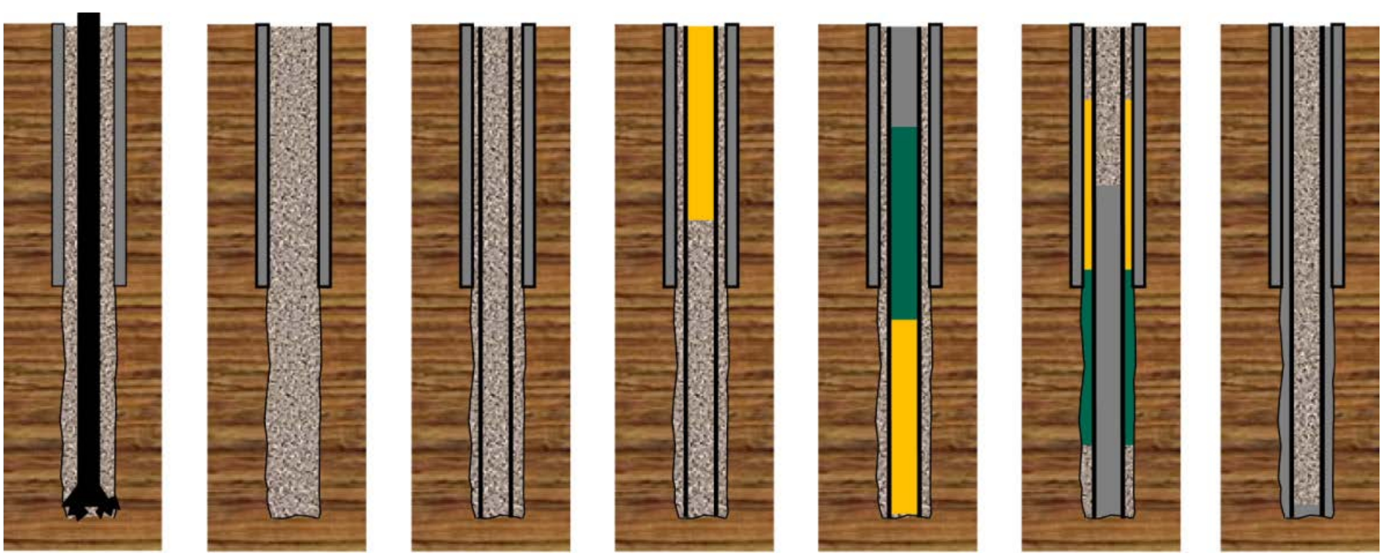

Figure 1: Schematics of primary cementing

An unsuccessful cement job allows the hydrocarbons to leak. Leakage during the primary cementing operation can lead to gas pockets and channels within the cement. Residual drilling mud in channels, layers or washouts can dry into porous material, the cement may shrink, later crack etc.. Thus, a number of defects may arise either during the cementing of a well, afterwards during cement hydration, or on longer timescales. The most common fluid-related defects include the following.

- **Residual mud channeling:** This is where the yield stress of the mud holds it in place, typically on the narrow side of the annulus, as preflushes and cement slurry by-pass in the wider parts of the annulus.
- **Wet micro-annulus:** This is a local mechanical effect, where the displacing fluid does not generate sufficient shear stress to mobilize the mud at the wall.
- **Mixing/contamination of the slurry:** Mixing (and consequent contamination) occur in different scenarios such as downwards displacement within the casing, fluid instabilities in laminar annular flows, or in turbulent annular displacement flows.

From a fluid mechanics perspective, one of the main operational questions is whether it is preferable to cement a well in turbulent or laminar flow. To explain this, displacement flow regime depends on local geometry and fluid properties as well as the overall imposed flow rate. It is relatively common within the annulus that one fluid can be fully turbulent (e.g. a chemical wash or low-viscous spacer) while others are laminar. Indeed, as it will be shown later, this also can occur on a single section of the annulus, e.g. turbulent on the wide side, laminar or even static on the narrow side. Furthermore, although some fluids can be strongly turbulent, the more viscous fluids (muds, viscous spacers and slurries) are often only weakly turbulent, transitional or laminar.

Project 1: Estimate of mixing in turbulent displacement flows

In this project, we consider 1D flows of a single Herschel-Bulkley fluid in a pipe or planar channel. The final objective is to provide some leading-order estimate for the turbulent diffusion as well as Taylor dispersion. To this end, we initially require an accurate profile of turbulent velocity in pipe or channel. Laminar velocity profiles are integrable from the constitutive law. For turbulent flows, the phenomenological method of Dodge-Metzner-Reed (Metzner and Reed, 1955; Dodge and Metzner, 1959) is popular in many process industries. In the context of dispersion, the Dodge-Metzner-Reed approach is attractive in that the hydraulic calculations (and closure) are linked to a universal log-law velocity profile, proposed by Dodge and Metzner (1959). However, in order to estimate Taylor dispersion, two common deficiencies must be dealt with: i) the symmetry condition at the centreline and ii) the no-slip condition at the wall. We explain this below.

Hydraulic framework

For pipe flows of power-law fluids, the Dodge-Metzner-Reed approach defines generalized Reynolds number as:

$$Re_{MR} = \frac{8^{1-n'}\rho W_0^{2-n'}}{k' D^{n'}}$$

where ρ is the fluid density and W_0 is the mean velocity. For power law fluids, the auxiliary variables n' and k' are given by

$$n' = n, k' = \left(\frac{3n+1}{4n}\right)^n$$

where n and k are power-law index and consistency. The complicated derivation of Re_{MR} has the virtue of ensuring that $f_f = 16/Re_{MR}$ in the laminar regime for all generalized Newtonian fluids. Here $f_f = 2\tau_W/\rho W_0^2$ is the friction factor and τ_w is the wall shear stress. For power law fluids, in all flow regimes, Re_{MR} is explicitly defined in terms of the mean velocity, making it straightforward to work with f_f, Re_{MR} and n in defining the mapping between τ_W and W_0. The simplicity of the Metzner-Reed formulation however is lost once we move more complex generalized Newtonian fluids and study different flow regimes. In particular, when the fluid has a yield stress, n' and k', and as a result Re_{MR}, will depend on both wall shear stress and mean velocity, which further complicates the hydraulic calculations. Ideally, we would like a Reynolds number to be solely dependent on the mean velocity, so we define:

$$Re_p = \frac{8^{1-n}\rho W_0^{2-n}}{k_p D^n}, k_p = \left(\frac{3n+1}{4n}\right)^n k$$

The other two dimensionless parameters we use are a dimensionless wall shear stress H_w and dimensionless yield stress (Hedström number) He as defined below:

$$He = \tau_Y \left(\frac{\rho^n D^{2n}}{k_p^2}\right)^{1/(2-n)}, H_w = \tau_w \left(\frac{\rho^n D^{2n}}{k_p^2}\right)^{1/(2-n)}.$$

The mapping $W_0 \leftrightarrow \tau_W$ can be stated in terms of Re_p, He, H_w and *n*. For laminar flows, this is given by:

$$\frac{(8Re_p)^{\frac{n}{2-n}}}{H_w} = E(n, r_Y)$$

and in turbulent flows

$$Re_p = H_w^{1-\frac{n}{2}} 2^{4-\frac{7n}{2}} \left[\frac{4}{n'^{0.75}} \log\left(2^{4-\frac{7n'}{2}} E(n, r_Y)^{\frac{n'}{n}} H_w^{\frac{n'}{n}-\frac{n'}{2}}\right) - \frac{0.4}{n'^{1.2}}\right]^{2-n}.$$

Here

$$r_Y = \frac{He}{H_w}, \quad E(n, r_Y) = (1 - r_Y)^{n+1} \left[(1 - r_Y)^2 + \frac{2(3n+1)(1 - r_Y)r_Y}{2n+1} + \frac{(3n+1)r_Y^2}{n+1}\right]^{\mathrm{n}} \text{ and}$$

$$n' = n(1 - r_Y)\frac{(n+1)(2n+1) + 2n(n+1)r_Y + 2n^2 r_Y^2}{(n+1)(2n+1) + 3n(n+1)r_Y + 6n^2 r_Y^2 + 6n^3 r_Y^3}.$$

The only missing piece here is a set of criteria for transition to turbulence. In Maleki and Frigaard (2016), we advocate for a two-tier criterion: i.e. a critical Reynolds number, $Re_1(n')$, which marks the loss of laminar regime and another critical number, $Re_2(n')$, which indicates a fully turbulent regime. The region in between is called transitional. The expressions for Re_1 and Re_2 are provided in Maleki and Frigaard (2016). Associated with these two values of critical Reynolds number, there are two critical wall shear stress values: $H_{w,1}(n, He)$ and $H_{w,2}(n, He)$. Figure 2 illustrates the 3 flow regimes in $H_w - Re_p$ and in $H_w - Re_{MR}$ spaces at $He = 500$ for $n = 0.2, 0.4, 0.6, 0.8$ and 1. We see large relative difference between Re_p and Re_{MR} at smaller values of n and H_w (laminar and transitional), which corresponds to those parameters where n' is smallest. Qualitatively similar plots are found at other He.

Turbulent velocity profile

Having designed our hydraulic frame work, we can now specify the profile of velocity. The derivation of this profile is explained in detail in Maleki and Frigaard (2016). In particular, two deficiencies are addressed: i) The log-law profile has a non-zero gradient at the centerline which violates the symmetry condition. ii) At the wall, the log-law profile does not satisfy the no-slip condition. In addition, the profile of turbulent stresses must decay cubically near the wall. We address (i) by introducing a correction term $B_{0,c}(r)$ and requiring the gradient of velocity must vanish at the centerline. To address (ii), we employed an asymptotic approach in constructing a *wall layer* velocity that meets the two conditions. Here we only outline the final result:

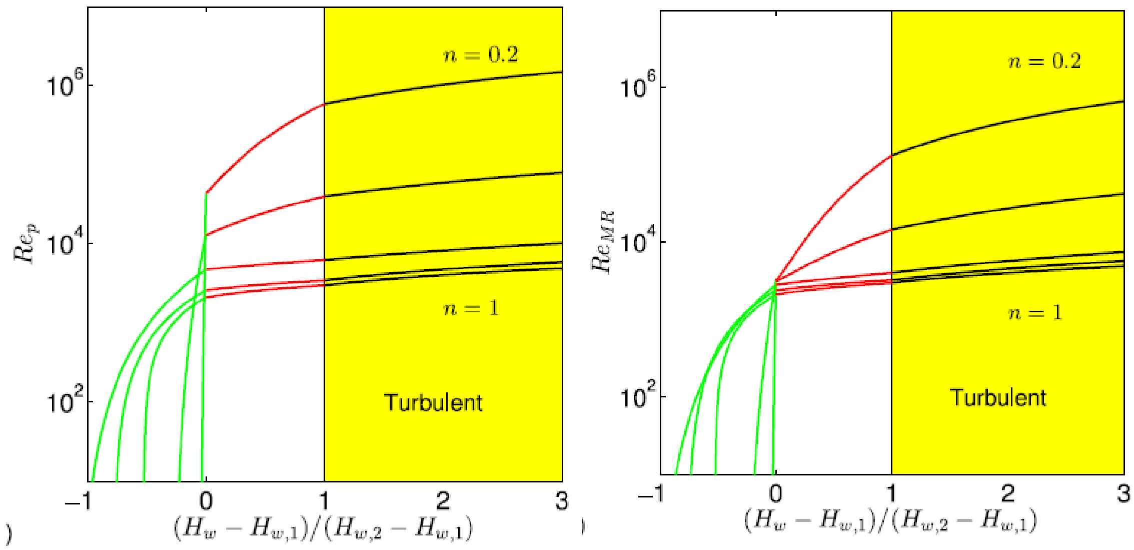

Figure 2: Plots of Re_p and Re_{MR} against $(H_w - H_{w,1})/(H_{w,2} - H_{w,2})$ for $He = 500$ and $n = 0.2,\ 0.4, \dots, 1$. Regimes are denoted: laminar (green), transitional (red), turbulent (black).

$$
\begin{cases}
W(r) = \sqrt{\dfrac{f_f}{2}}\left[A_0 \ln(1-r) + B_0 + B_{0,c}(r)\right] & 0 \le r \le r_c \\
W(r) = \displaystyle\sum_{i=0}^{5} a_i (R-r)^i & r_c \le r \le R
\end{cases}
$$

where

$$
A_0 = \frac{4\sqrt{2}}{\ln 10} n'^{0.25}, B_0 = -\frac{0.4\sqrt{2}}{n'^{1.2}} + A_0\left(\frac{1}{n'}\ln\left(f_f^{1-\frac{n'}{2}} Re_{MR}\right) + \frac{3}{2}\right), B_{0,c}(r) = A_0\left(r(1-r)^2 - \frac{1}{15}\right)
$$

The coefficient a_i's as well as the critical radius r_c can be calculated by solving a complex system of non-linear equations. Please refer to Maleki and Frigaard (2016).

Figure 3 plots the turbulent velocity profile for $He = 100$ and $n = 0.2, 0.4, \dots, 1$. The wall shear stress is $H_w = 1.05\ H_{w,2}$, i.e. just enough to have a fully turbulent regime. Notice that the velocity profile has a logarithmic shape in the core with a correction function ($B_{0,c}$) that provides a zero gradient at the centreline (symmetry condition). The wall profile (red lines) ensures that the no-slip condition is satisfied. Similar to laminar velocity profile, as the fluid becomes more shear thinning, the profile of velocity is flatter. In addition, the wall layer thickness is vanishingly small at low values of n.

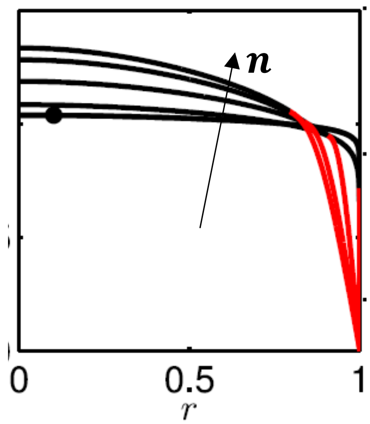

Figure 3: Profile of velocity for $He = 100$, $n = 0.2,\ 0.4, \ldots, 1$ and $H_w = 1.05\ H_{w,2}$. Wall layers are denoted with red.

Turbulent diffusion and Taylor dispersion estimation

Estimation of turbulent diffusion and Taylor dispersion is possible using the Reynolds analogy which allows to write the turbulent diffusion (D_t) as in terms of eddy diffusivity (D_e) and turbulent Schmidt number (Sc_t):

$$D_t = \frac{1}{Sc_t} D_e = \frac{1}{Sc_t \rho \left|\frac{\mathrm{d}W}{\mathrm{d}r}\right|}\left(\frac{r}{R}\tau_W - |\bar{\tau}_{rz}|\right)$$

We can now estimate the average viscous shear stress ($\bar{\tau}_{rz}$) and the velocity profile obtained earlier to calculate turbulent diffusion coefficient. Upon finding the turbulent diffusion coefficient, the Taylor dispersion coefficient can be computed by

$$D_T = \frac{1}{2}\int_0^R \frac{\left(\int_0^r [W(s) - W_0]s\,\mathrm{d}s\right)^2}{r(D_t + D_m)}$$

Figure 4a plots the profile of turbulent diffusion. The parameters here are exactly those in Figure 3. The red lines show the contribution of wall layers. In Maleki and Frigaard (2016), we demonstrate the correction procedure we followed to find a more accurate profile of velocity has a major effect on the profile of turbulent diffusion. Figure 4b plots the profile of Taylor dispersion coefficient as a function of wall shear stress when $He = 100$. The horizontal axis is scaled such that 0 indicates onset of turbulent. We observe the dispersion coefficient is 2 to 3 orders of magnitude larger than turbulent diffusion. In addition, Taylor dispersion is larger when the flow is only weakly turbulent. As the flow become more turbulent, or as the shear thinning index drops down, the magnitude of Taylor dispersion coefficient decreases. Finally, in Figure 4c, we have compared our results together with the original results of Taylor (1954) as well as number of experimental data for Newtonian fluids. It can be seen that our estimate is close to the experimental measurements.

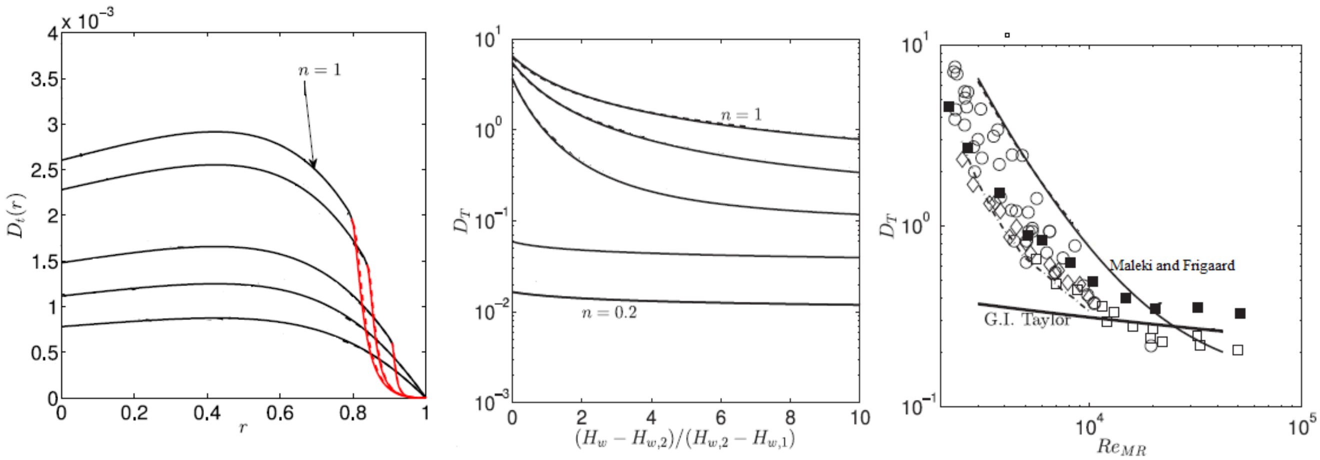

Figure 4: a) Profile of turbulent diffusion coefficient for $He = 100$, $n = 0.2,\ 0.4, \ldots, 1$ and $H_w = 1.05\ H_{w,2}$. Wall layers are denoted with red. b) Profile of Taylor dispersion coefficient as a function of wall shear stress. c) Comparison of different profiles of Taylor dispersion coefficient obtained analytically (solid lines) and experimentally (symbols).

Key results

The key results of this project can be summarized as below.

1. Although the Dodge-Metzner-Reed hydraulic calculation framework has some advantageous features, its utility is lost when working with yield stress fluids. We instead modified this framework such that the mapping $\tau_W \leftrightarrow W_0$ can be described by $Hw \leftrightarrow Re_p$.

2. We have extended the classical Taylor dispersion to shear-thinning yield stress fluids. We show that to find the Taylor dispersion coefficient, a *corrected* velocity profile is necessary. The corrections address the deficiencies of log-law velocity profile near the centerline and near the wall. Our results show that the wall layer correction significantly influences the Taylor dispersion coefficient.

3. Additionally, we found that although the yield stress produces competing effect in the wall layer, because of friction factor closure and delayed transition, the thickness of wall layer decreases as the yield stress drops. Similar behavior is also observed, not surprisingly, when the fluid becomes more shear thinning. Therefore, the dispersion is suppressed as power-law index is reduced or yield stress is increased.

4. Most importantly, we found that in weakly turbulent flows the mixing due to the Taylor dispersion is one or two orders of magnitude larger than that of turbulent diffusion.

The results presented above were all obtained for flow in a pipe. We have performed similar analysis for flow in a planar channel and obtained analogous expressions. For the sake brevity of this report, we do not repeat these results and we refer to Maleki and Frigaard (2016).

Project 2: Multi-regime annular displacement model

Model summary

Project 2 is core of our work. Here, we derived a 2D model for the displacement of shear-thinning yield stress fluids in eccentric annular geometries. The key assumption in this derivation is the narrow-gap approximation; i.e. we assume the annular gap is significantly smaller the average circumference of the annulus. The narrow gap approximation justifies averaging the variation in the radial direction and reducing the problem into 2D. In addition, we find that to the leading-order, the narrow gap approximation simplifies the momentum equations to a turbulent shear flow in the direction of the modified pressure gradient.

Upon averaging in the radial direction, we unwrap the annulus into a 2D planar space of (ϕ, ξ) where ϕ is the azimuthal coordinate and ξ is the axial coordinate. The 2D model consists of an elliptic equation for the streamfunction:

$$\boldsymbol{\nabla}_{\mathbf{a}}.\left(\frac{\tau_w(|\nabla_{\mathrm{a}}\Psi|)}{H|\nabla_{\mathrm{a}}\Psi|}\nabla_{\mathrm{a}}\Psi + \mathbf{b}\right) = 0$$

and an advection-diffusion-dispersion equation for the concentration of each fluid:

$$\frac{\partial c_k}{\partial t} + (v,w).\nabla_a c_k = \frac{\delta_0}{\pi}\left(\boldsymbol{e_s}.\nabla_a[D_T\,\boldsymbol{e_s}.\nabla c_k] + \frac{1}{2H}\boldsymbol{\nabla_a}.[2H\,D_t\nabla c_k] + \frac{1}{H}(\boldsymbol{e_s}.\nabla_a H)(\boldsymbol{e_s}.\nabla_a c_k)(D_T - D_T^*)\right)$$

Here Ψ is the streamfunction, and c_k is the concentration of fluid k which varies from 0 (absence of fluid k) to 1 (entirely fluid k). The two geometrical variables r_a and H denote the dimensionless mean radius and the dimensionless half-width of the annulus. The buoyancy vector $\boldsymbol{b}$, which is a source term for the streamfunction equation, is defined by

$$\boldsymbol{b} = \frac{r_a(\hat{\rho} - 1)}{Fr^2}(\cos\beta\,, \sin\pi\phi\,\sin\beta)$$

where $\hat{\rho}$ is the dimensionless density, β is the inclination angle (measured from vertical) and Fr is the Froude number. The operator ∇_a is the annular version of ∇, defined below:

$$\nabla_a f = \left(\frac{1}{r_a}\frac{\partial f}{\partial\phi}, \frac{\partial f}{\partial\xi}\right), \quad \text{and} \quad \boldsymbol{\nabla}.\boldsymbol{f} = \left(\frac{1}{r_a}\frac{\partial \boldsymbol{f_\phi}}{\partial\phi} + \frac{\partial \boldsymbol{f_\xi}}{\partial\xi}\right).$$

After solving the equation for the streamfunction, we recover velocity field by differentiating streamfunction:

$$(v,w) = \frac{1}{2H}\left(-\frac{\partial\Psi}{\partial\xi}, \frac{1}{r_a}\frac{\partial\Psi}{\partial\phi}\right)$$

where v and w and the gap-averaged azimuthal and axial velocity components, respectively. The velocity field is used to compute the diffusion (D_t) and dispersion (D_T, D_T^*) coefficients, as described in Project 1.

Numerical Algorithm

An important aspect of this project was to design a robust computational algorithm for solving the model. The necessity of a robust computational algorithm arises from the yield stress nature of the fluids and potentially multi-regime nature of flow. More specifically, in an eccentric annulus, the flow is faster on the wide side and slower on the narrow side, which means the flow regime can transition from turbulent on the wide side to laminar on the narrow side. In more extreme cases, the wall shear stress on the narrow side does not exceed the fluid yield stress and as a result, the fluid on the narrow side remains stuck, forming a mud layer. In order to correctly identify the position of mud layers, the viscoplastic behavior of the fluids has to resolved. To this end, we designed an algorithm that can be categorized as an augmented Lagrangian algorithm. These algorithms are highly reliable in simulating viscoplastic flows. For more details of the algorithm, please refer to Dr. Maleki's PhD thesis (Maleki, 2019).

Example of a displacement simulation

Figure 5 shows an example of a displacement simulation. In the left sub-figure, we have snapshots of displacement at different times. Recall that we reduce the radial variations through averaging and unwrap the annulus in a (ϕ, ξ) planar space. The horizontal axis denote the azimuthal coordinate, where $\phi = 0$ indicates the wide side of the annulus and $\phi = 1$ indicates the narrow side of the annulus. Clearly, $\phi = 2$ is again the wide side. The vertical axis is the axial coordinate, where $\xi = 0$ denotes the bottom of the annulus. In the simulations presented in the report, the annulus is initially field with the displaced fluid (here red fluid). At $t = 0$, the displacing fluid is pumped into the annulus at a prescribed flow rate. The right sub-figure shows a map of displacement regime. Here white, light gray and dark gray represent regions with fully turbulent, transitional and laminar regime. The regions highlighted in black are unyielded, i.e. fluid that does not move. In the well this is typically a mud channel.

In the Example shown in Figure 5, the annulus has inner and outer radius of $r_i = 16.5\ \mathrm{cm}$ and $r_o = 19\ \mathrm{cm}$. The annulus is vertical and has an eccentricity of $e = 0.5$. The displaced (sub-index 1) and displacing (sub-index 2) fluids have the following properties:

$$\rho_1 = 1200\frac{\mathrm{kg}}{\mathrm{m}^3}, n_1 = 1, \kappa_1 = 0.005\ \mathrm{Pa.s}, \tau_{Y,1} = 8\ \mathrm{Pa.s} \quad \text{and} \quad \rho_2 = 1300\frac{\mathrm{kg}}{\mathrm{m}^3}, n_2 = 0.7, \kappa_2 = 0.034\ \mathrm{Pa.s}^{0.7}, \tau_{Y,2} = 0\ \mathrm{Pa.s}$$

The flow rate here is $Q = 0.0426\ \mathrm{m}^3/\mathrm{s}\ (= 16.38\ \mathrm{bbl/min})$ which is equivalent to a mean velocity of $W_0 = 1.5\ \mathrm{m/s}$.

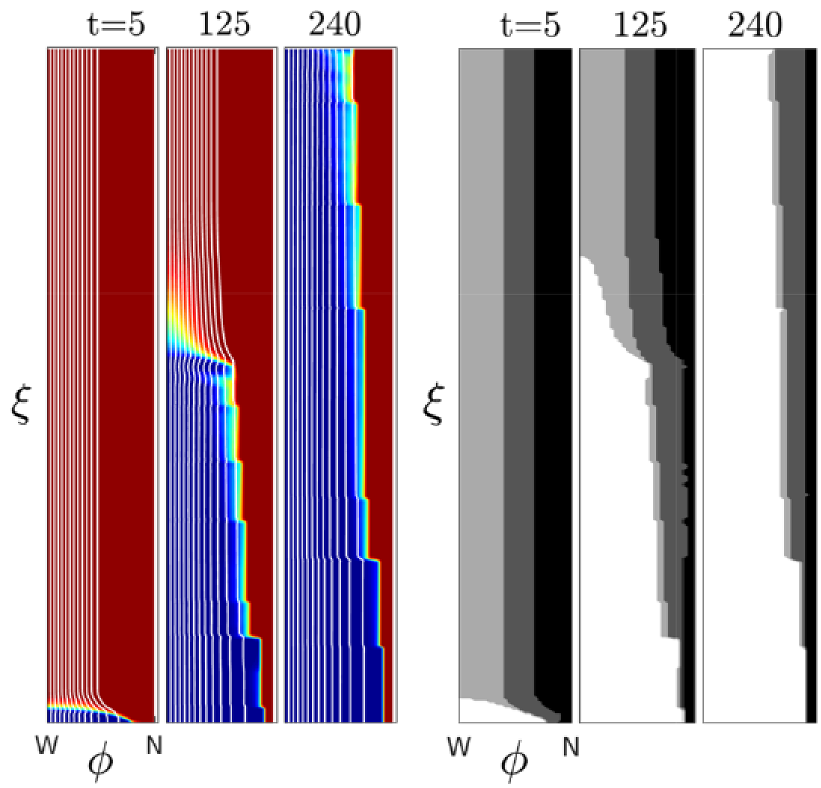

Figure 5: Example of a displacement simulation. Left) Snapshots of displacement at difference times. Well, geometry, fluid properties and flow rates are mentioned in the text. Time is reported dimensionlessly. Right) Map of displacement regime. See the text of the interpretation of colors.

Case studies

The effect of rheological parameters in turbulent displacement

Our first case study establishes a principle that we will refer to frequently later. The principle states as long as the displacement regime is fully turbulent, the rheology of the fluids does not have any significant influence on the displacement outcome. Notice that the rule applies as long as the displacement remains fully turbulent. If after the rheological parameters (say the viscosity), the displacement falls into the laminar regime, then the rheology become important again. To illustrate this point, let us consider the following example: Consider the annulus of Figure 5 that is initially filled with a Newtonian fluid with $\rho_1 = 1200 \text{ kg/m}^3$ and $\mu_1 = 0.001 \text{ Pa. s}$. Three choices of displacing fluids all with density $\rho_2 = 1250 \text{ kg/m}^3$ are tested:

$$\text{Fluid A}: n_2 = 1.0, \kappa_2 = 0.0010 \text{ Pa. s and } \tau_{Y,2} = 0 \text{ Pa.}$$

$$\text{Fluid B}: n_2 = 0.7, \kappa_2 = 0.0024 \text{ Pa. s and } \tau_{Y,2} = 0 \text{ Pa.}$$

$$\text{Fluid C}: n_2 = 0.4, \kappa_2 = 0.0059 \text{ Pa. s and } \tau_{Y,2} = 0 \text{ Pa.}$$

The prescribed flow rate is $Q = 0.0142 \text{ m}^3/s$ (or equivalently $W_0 = 0.5\ m/s$) at which these three fluids generate (nominally) same frictional pressure loss. The displacement snapshots are shown in Figure 6. Clearly, the change of rheological parameter had no influence on the displacement outcome. More quantitatively, the difference of axial velocity in these three cases is of order of the simulation truncation error (10^{-5}). In addition, in Maleki and Frigaard (2018b), we analyzed this example in more details. In particular, we show if we reduce the flow rate so much that the displacement become laminar, the rheology appears to be influential again. Furthermore, we showed if even one of the fluids become laminar, then the displacement begins to depend on rheological parameter of either of fluids (and not necessarily the laminar fluid).

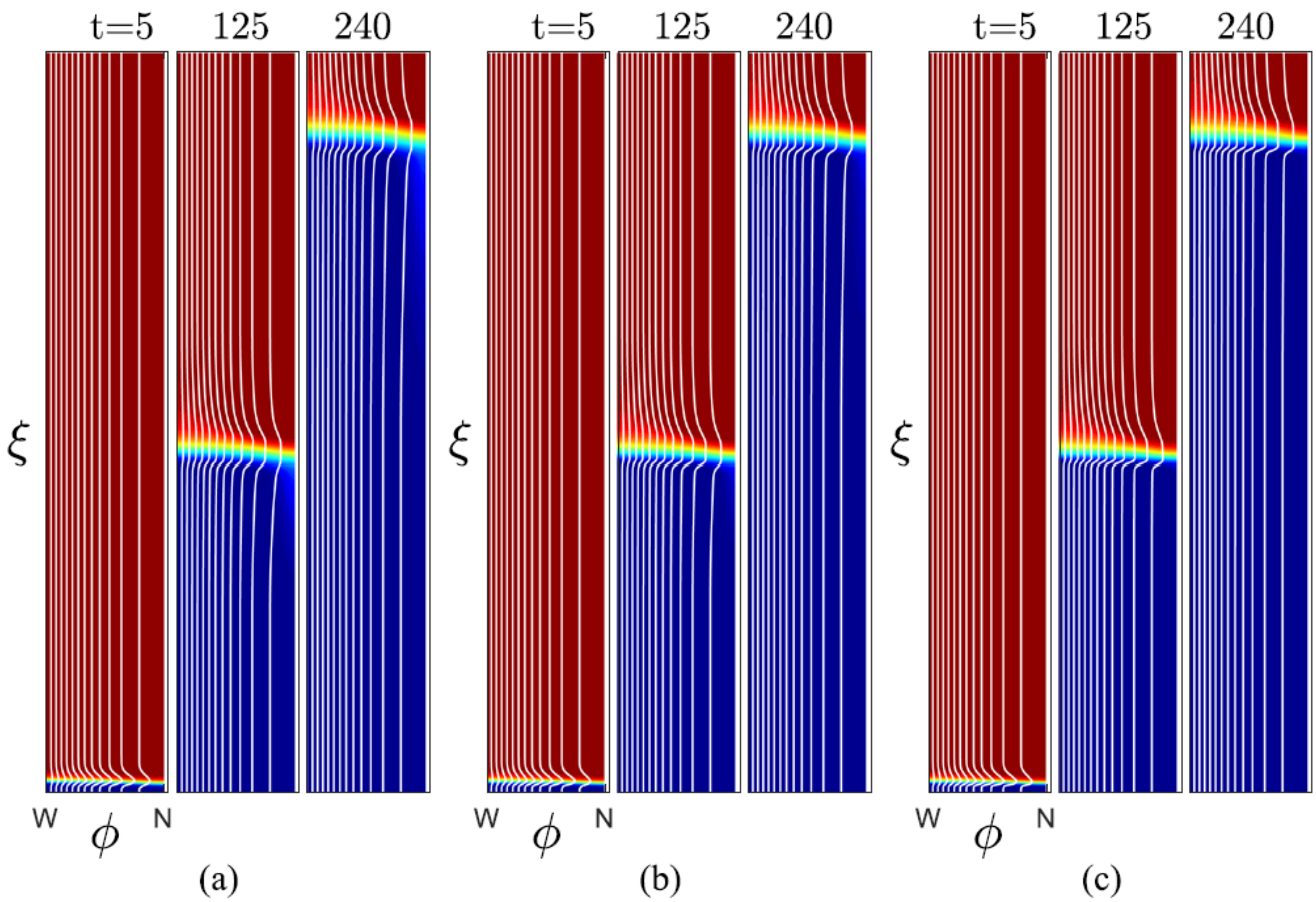

Figure 6: Demonstration of the effect of rheological parameter on the fully turbulent displacements. a) Fluid A; b) Fluid B and c) Fluid C. See the text for the details of the displacement cases.

The implication of this principle is that controlling turbulent displacement flows and ensuring steady displacement are more difficult than with laminar displacement flows because in laminar flows one can play with both the viscous and buoyancy forces to ensure a steady displacement. In turbulent flows however, the only tool left is buoyancy forces. For example, in highly inclined and horizontal wells, turbulent flows are likely to be unsuccessful at removing the mud from eccentric annuli.

The effect of buoyancy in turbulent displacement

In an eccentric well, the flow tends to be faster on the wide side, simply because in a narrow annulus the wall shear stress scales linearly with the gap width: a larger wall shear stress induces a larger gap-averaged velocity. For the very same reason, the displacement is slower on the narrow side. It is perhaps astonishing that when this same feature is present both far downstream and far upstream of an "interface", the interface may itself propagate at uniform (mean) speed along the annulus. In the laminar flow, steady displacements arise via positive gradients of density and frictional pressure. In turbulent flows, we just established that rheology is not very important and it is only the buoyancy that can stabilize a turbulent displacement. In Maleki and Frigaard (2018b), we demonstrate that his stabilizing mechanism happens through development of counter-clockwise flows near the interface. These secondary flows move the displacing fluid to the narrow side and the displaced fluid to the wide side. This mechanism clearly competes against the bias that eccentricity creates in the flow and is the source of stabilization.

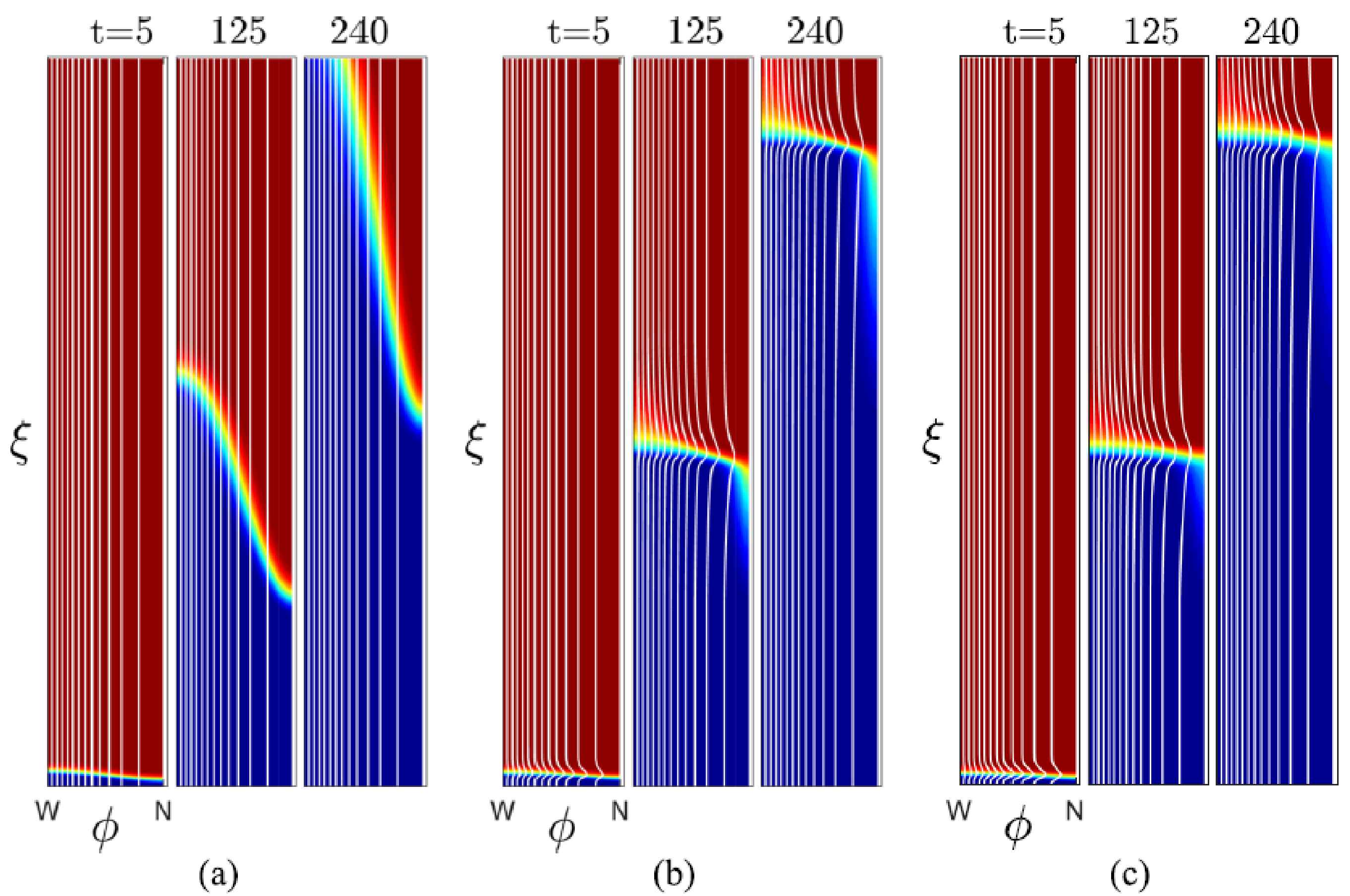

Figure 7: Demonstration of the effect of density difference on the fully turbulent displacements. a) $\rho_2 = 1200\ kg/m^3$A; b) $\rho_2 = 1215\ kg/m^3$ and c)) $\rho_2 = 1230\ kg/m^3$. See the text for the details of the displacement cases.

To illustrate this in the context of a real displacement scenario, we consider the example presented in Figure 6a, except we vary the displacing fluid density. Staring from no density difference ($\rho_1 = \rho_2 = 1200\ \mathrm{kg/m^3}$ in Figure 7a), we then gradually increase the displacing fluid density to $\rho_2 = 1215\ \mathrm{kg/m^3}$ (Figure 7b) and then $\rho_2 = 1230\ \mathrm{kg/m^3}$ (Figure 7c). In Figure 7a, the two fluids have identical densities. With no stabilizing density difference, the interface elongates. As we introduce the density difference in Figures 7b and 7c, the interface velocity becomes progressively uniform around the annulus. Elongation of the interface is suppressed, and the flow is more steady. Turbulent displacement flows are of course dispersive by nature: the interface continuously diffuses along the streamlines via Taylor dispersion (see Project 2). Thus, strictly speaking, the interface will always be unsteady and spread. Nonetheless, turbulent flows can still be steady in the sense that the interface moves uniformly around the annulus. This can be demonstrated by measuring the differential velocity ($w_W - w_N$). In Maleki and Frigaard (2018b), we showed that the examples of Figures 7a and 7b are not steady, as a positive differential velocity pertains at the interface. Whereas, for Figure 7c, the differential velocity vanishes at the interface, suggesting that the interface is perfectly steady.

Loss of steady displacement when the flow is highly turbulent

In the cementing community it is widely believed that the more turbulent the flow, the more efficient the displacement. However intuitively, as the flows becomes more turbulent (e.g., by increasing the flow rate), the turbulent wall shear stress increases and eventually dominates the flow, rendering both rheology and density differences unimportant in the displacement. As a result, no mechanism remains present in the displacement flow to make the displacement front steady. Therefore, one would expect the displacement to become unsteady. In Maleki and Frigaard (2018b), we investigated this scenario at length. We demonstrated that examples of a perfectly steady turbulent displacement can turn unstable if the flow rate is increased too much. We call this regime "too turbulent", meaning that the flow is so turbulent that the stabilizing effect of buoyancy is lost. In order to characterize the notion of "*too turbulent*", we define a dimensionless parameter, the turbulent Richardson number:

$$Ri = \frac{(\rho_2 - \rho_1) g (r_o - r_i)}{\frac{1}{2}\rho_1 W_0^2 f_f}$$

The numerator is a representative magnitude of buoyancy force and the denominator is representative magnitude of turbulent stress. (Recall that f_f is the friction factor, defined in Project 1). Therefore, Richardson number is the ratio of buoyancy stresses to turbulent stress. As the flow becomes more turbulent, the Richardson number decreases, so we expect the regime of "*too turbulent*" happens at lower values of Richardson number. To understand this more clearly, we have conducted a parametric study and summarized the results in Figure 8. Here, we vary eccentricity and flow rate (and consequently Richardson number) and record if the displacement is steady (green symbols) or unsteady (red symbols). For this particular example, it appears that the criterion to avoid *too turbulent* flows is simply given by

$$Ri \geq 1.$$

In other words, if the turbulent stress scales are larger than a representative buoyancy stress, then the flow becomes too turbulent and therefore unsteady. Another interesting regime identified in Figure 8 is the too eccentric regime. It appears for $e \geq 0.6$, regardless of the value of Richardson number (i.e. regardless of density difference), the displacement is unsteady. This means that for a given stabilizing density difference there is a limiting eccentricity that can be overcome.

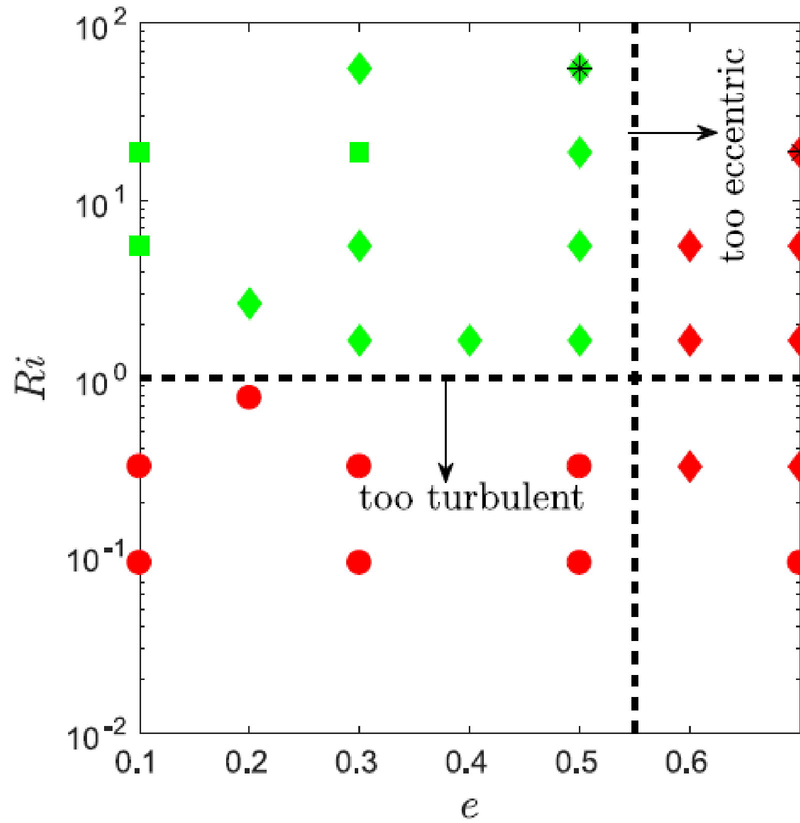

Figure 8: Displacement outcome as a function of eccentricity and Richardson number. Red and green symbols indicate unsteady and steady displacement. Circles indicate fully turbulent displacement. Diamonds and squares are mixed flow regime.

It is worth mentioning here that although the criterion above is a useful prediction, we need to be a little cautious about its generality and that of Figure 8. We constructed this example by increasing Richardson number through lowering the flow rates—leading eventually to laminar flows. An alternate would be to vary the density difference at a fixed flow rate and probably there are other possibilities. However, in principle, Figure 8 could be constructed for any pair of fluids and annulus.

Comparison of laminar and turbulent displacement

One of the key goals of Project 3 was to compare laminar and turbulent displacement flows in terms of their outcome. The early literature on cementing generally stated that turbulent displacement is more successful than those in laminar regime in removing the mud during primary cementing; see for example Sauer (1987), Nelson (1990), Kettl et al. (1993). While some recent studies have been less definitive and warned that certain conditions must be satisfied for turbulent displacement to succeed, e.g. Nelson and Guillot (2006), Khalilova et al. (2013), there still appears to be a widely accepted perception in the cementing community that turbulent displacement is necessarily superior to laminar displacement; see for example Lavrov and Torsater (2016), Enayatpour and van Oort (2017). Despite its popularity, the scientific evidence to support this notion is scant. In Maleki and Frigaard (2019), we have extensively reviewed the literature pertinent to this claim. In summary, to our knowledge, there is no objective study that compares cementing displacement flows in both laminar and turbulent regimes, within operational constraints.

Here we consider the problem of defining a reasonable comparative test case for cementing of a vertical casing. Primary cementing presents some difficulties in terms of defining typical data, which it is worth remarking on. As with many industrial processes, effective data recording and analysis is a precursor to process improvement. Unfortunately, many parameters of importance to the effectiveness of primary cementing, namely eccentricity, rheological parameter as well as pumping schedule, are not evaluated or recorded in any easily accessible format. In addition to the lack of sensitive data, the variability is also of great importance. For example, the diameter of an annulus can start at anything around 50 cm at the top of surface casing, and tapers down to about 10 cm at the bottom of production casing. In Maleki and Frigaard (2019), we have surveyed the recent literature and extracted a long list of primary cementing parameters. In our example, we will use values representing typical scenarios of displacement.

Another important consideration is the operational constraints. We recall that primary cementing is constrained by the formation fracture pressure and the pore pressure (the pore-frac envelope), i.e. to retain primary well control. This constrains the densities used and also the flow rates. Any well will have its own specific limits. Here we just wish to emphasize that such a constraint exists and explore its effects. Loosely speaking, this is a frictional pressure constraint, which in practice is to be satisfied at each position in the open-hole and at each time through the operation. To simplify this, we simply impose that the total frictional pressure drop generated by the displacing fluid, over the length of well, down the inside of the casing and up in the annulus, should be less than 150 psi (= 1034 kPa). The value 150 psi is representative of a typical safety margin, but is otherwise nominal for the 500m well we consider. We use the hydraulic framework of Project 2 to calculate the maximum flows rate possible without violating the 150 psi constraint.

In this report, we only present one of the examples. Interested readers can refer to Maleki and Frigaard (2019) for more examples and more detailed discussion. Consider a 500 m-deep annulus with inner and outer radii of $r_i = 16.5\ \mathrm{cm}$ and $r_o = 19\ \mathrm{cm}$ and eccentricity $e = 0.6$. The annulus is initially filled with a drilling mud with properties:

$$\rho_1 = 1200\,\frac{\mathrm{kg}}{\mathrm{m}^3}, n_1 = 1, \kappa_1 = 0.01\ \mathrm{Pa.s}, \tau_{Y,1} = 10\ \mathrm{Pa.s}$$

The yield stress here is significant, i.e. this is not a trivial fluid to displace. Five fluids with different properties are listed below. For each of these fluid candidates, the maximum flow rate without violating the frictional pressure loss constraint is computed.

$$\text{Fluid A}_1\text{:}\quad \rho_2 = 1350\,\frac{\text{kg}}{\text{m}^3}, n_2 = 1, \kappa_2 = 0.04\ \text{Pa.s}, \tau_{Y,2} = 0\ \text{Pa.s} \ \text{ with a flow rate of } Q = 0.039\,\frac{\text{m}^3}{\text{s}},$$

$$\text{Fluid A}_2\text{:}\quad \rho_2 = 1350\,\frac{\text{kg}}{\text{m}^3}, n_2 = 1, \kappa_2 = 0.01\ \text{Pa.s}, \tau_{Y,2} = 0\ \text{Pa.s} \ \text{ with a flow rate of } Q = 0.043\,\frac{\text{m}^3}{\text{s}},$$

$$\text{Fluid A}_3\text{:}\quad \rho_2 = 1350\,\frac{\text{kg}}{\text{m}^3}, n_2 = 0.5, \kappa_2 = 0.3\ \text{Pa.s}^{0.5}, \tau_{Y,2} = 2\ \text{Pa.s} \ \text{ with a flow rate of } Q = 0.043\,\frac{\text{m}^3}{\text{s}},$$

$$\text{Fluid } B\text{:}\quad \rho_2 = 1350\,\frac{\text{kg}}{\text{m}^3}, n_2 = 1, \kappa_2 = 0.001\ \text{Pa.s}, \tau_{Y,2} = 0\ \text{Pa.s} \ \text{ with a flow rate of } Q = 0.039\,\frac{\text{m}^3}{\text{s}},$$

$$\text{Fluid } C\text{:}\quad \rho_2 = 1350\,\frac{\text{kg}}{\text{m}^3}, n_2 = 1, \kappa_2 = 0.040\ \text{Pa.s}, \tau_{Y,2} = 5\ \text{Pa.s} \ \text{ with a flow rate of } Q = 0.016\,\frac{\text{m}^3}{\text{s}},$$

Figure 9 shows the displacement snapshots together with the regime maps for each of these five displacing fluid candidates. We observe that the flow regime is transitional for Fluid A_1 and partially turbulent for Fluids A_2 and A_3. In all cases however, the mud remains either in laminar or at most transitional regime, due to its larger yield stress. The change in the flow regime, both axially along the well and azimuthally around well is clearly depicted here. Despite the change in the flow regime from laminar and transitional in the case of Fluid A_1 to turbulent in the case of Fluids A_2 and A_3, the displacement outcome does not appear to have improved significantly.

The displacement with Fluids A_1, A_2 and A_3 are all unsteady, meaning that the interface is faster on the wide side and slower on the narrow side. This leads to continuous elongation of the interface and accumulation of mud that is left behind on the narrow side. Ideally, we would like to avoid this. Two different directions may be pursued to improve the displacement efficiency: i) reduce the viscosity of the spacer and enhance turbulence (Fluid B) or ii) increase the yield stress of the spacer and rely on viscoplastic stresses (Fluid C). The displacement snapshots for these two choices are shown in Figures 9d and 9e. In case of Fluid B (Figure 9d) the turbulent regime expands and is now found all around the annulus within Fluid B. The interface is still progressing unsteadily, however the wide and narrow side velocity difference has shrunk slightly, as can be seen by the large volume of mud that is displaced on the narrow side. The displacement is of course improved, which appears to be due to the turbulent regime. On the other hand, for Fluid C, the displacement has deteriorated, as the mud on the narrow side barely moves. We note that neither displacement was effective. In particular, the common notion that a turbulent flow will spread around the annulus is not found to be true in the case of high eccentricity.

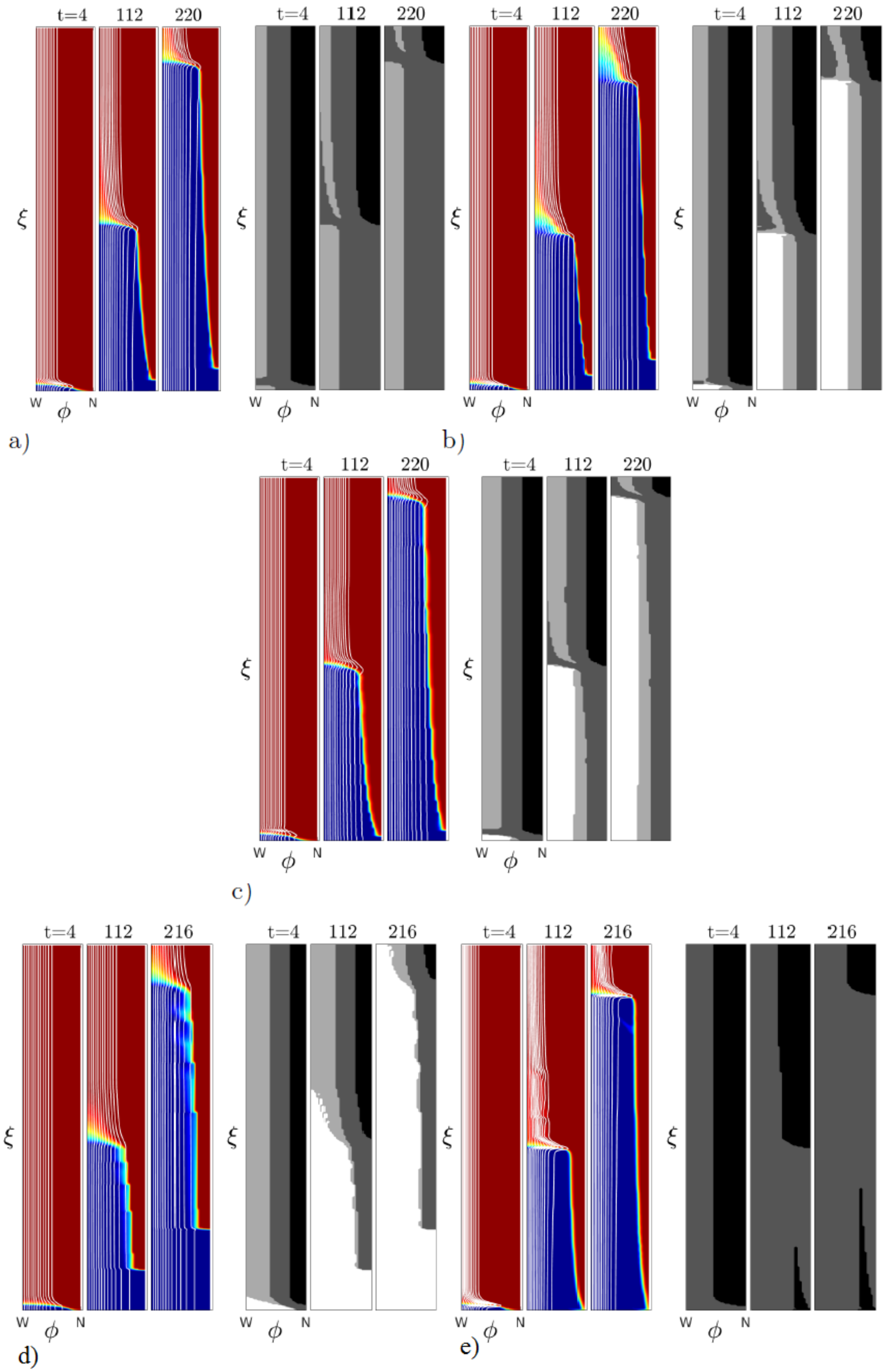

Figure 9: Demonstration of the effect of flow regime on the displacement outcome. a) Fluid A_1 ; b) Fluid A_2 ; c) Fluid A_3; d) Fluid B and e) Fluid C. See the text for the details of the displacement cases. In each case, the left sub-figure shows the displacement snapshots and right sub-figure shows the regime map. White, light gray and dark gray and black regions indicate turbulent, transitional, laminar and unyielded flow regimes.

To compare the performance of the five displacing fluid candidates more quantitatively, it is customary in the literature to quantify the displacement using a volumetric efficiency $\eta(t)$, which is the percentage of mud that is displaced. The above definition of efficiency might be somewhat deceptive, in that although quantitative, it gives a biased impression of how effective a cement job is. This is because the volume of annulus on the narrow side is smaller than on the wide side. Therefore, when the mud on the wide side is displaced successfully, as is commonly the case, the value of volumetric efficiency grows rapidly. This happens despite having mud left behind on the narrow side. From the perspective of well leakage, a residual mud channel is a severe problem. As an example, for an annulus with e = 0:6, the widest quartile of annulus has a volume 3.25 times larger than that of the narrowest quartile. As a result of this azimuthal bias, the value of volumetric efficiencies can easily reach as high as 80-90%, even if the displacement is poor on the narrow side. In fact, this is the case for the displacement example shown in Figure 9. Figure 10a plots the volumetric efficiency as a function of (dimensionless) time (t) for all the five displacing fluid candidates. Although none of displacement examples can be called successful, as is clearly illustrated in Figures 9, the efficiency values are as high as 90%.

To account for the above bias, we define narrow side displacement efficiency (η_N) which calculates the efficiency only in the narrowest quartile of the annulus. Figure 10b plots the narrow side displacement efficiency $\eta_N$vs time for all the five fluid candidates in figure 8. As expected, the narrow side efficiency reflects a better picture of the displacement quality. We observe roughly two-third of the mud in the narrowest quartile of the annulus is left behind. The highest efficiency around 35%. Interestingly, the laminar displacement (Fluid C) performed almost equally as well as the partially turbulent displacements (Fluids A1 and A2), and the fully turbulent displacement (Fluid B).

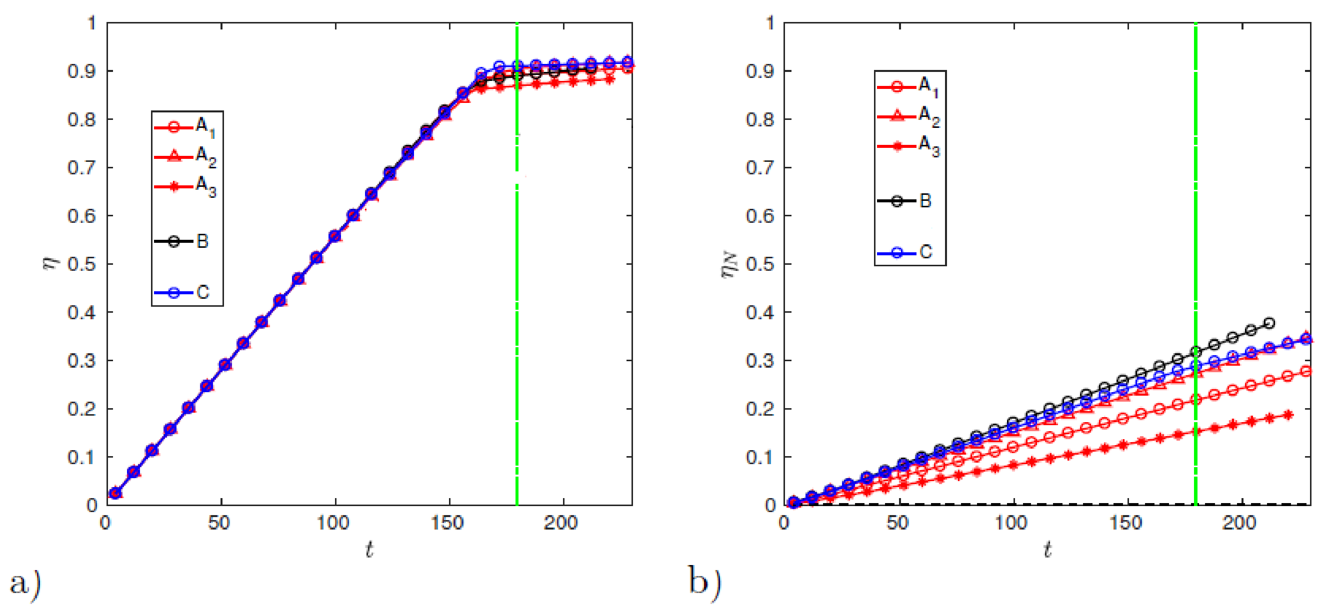

Figure 10: Displacement efficiency as a function of (dimensionless) time for the example of Figure 9. a) displacement efficiency η; b) narrow side displacement efficiency η_N

Upon closer inspection, it appears that the single parameter that has made the displacement examples above unsuccessful is the eccentricity of the annulus. To elucidate the critical role of eccentricity, in Maleki and Frigaard (2019) we have repeated the above simulations for slightly less eccentric annuli: $e = 0.4$ and $e = 0.3$. We confirmed that the narrow side displacement efficiency has improved significantly when the well is less eccentric. For example, when $e = 0.3$, Fluids A_1, A_2, B and C reach a narrow side displacement efficiency of > 95%.

Displacement of low viscous light-weight preflush (wash)

In order to avoid contamination and ensure a good cement bond it is imperative that drilling fluids are removed from the annulus during primary cementing. After an amount of mud conditioning during the pre-circulation phase, a typical fluid sequence consists of one or more preflushes pumped ahead of the cement slurries in the annulus. Preflushes can be generally divided into two categories: I) Light weight, low viscosity preflushes known as washes and II) weighted and viscosified preflushes known as spacers. This case study primarily concerns the first of these.

Washes may be water-based or oil-based. Rheologically, they are generally Newtonian fluid solutions (e.g. water). They are designed to wash the walls of the annulus free from residual fluids (and any remaining solids), to leave the annulus water- wet for the cement slurry. In addition, they should break any static gelation of the mud, mobilizing the mud in general. The low viscosity and density of these fluids allows them to be pumped in turbulent flow regimes. Turbulent displacement is believed to be more effective in terms of cleaning the annulus walls (Nelson and Guillot, 2006 and Lavrov and Torsater, 2016). In using a wash, cementing protocols suggest that a minimum contact time is met. The contact time here refers to the time taken for the wash to pass a position in the annulus. Typically, this minimum contact time is 10 minutes, although shorter contact times (e.g. 5 minutes) may be recommended when the flow is fully turbulent (Nelson and Guillot, 2006).

The objective of this case study is to analyze the displacement using washes. More specifically, do the washes really mobilize the mud? Does the turbulent flow regime enhance the displacement? How accurate is the 10-minute contact time as a measure of cleaning provided by the wash.

Consider a surface casing displacement scenario with inner and outer radii of $r_i = 24.5\ \mathrm{cm}$ and $r_o = 31\ \mathrm{cm}$. The depth of the surface casing is *450* m and its eccentricity is only $e = 0.3$; in other words, the annulus is pretty well centralized. Our examples in this case studies involve three fluids: a drilling mud (index 1), a preflush (index 2) and a cement slurry (index 3) with the following properties

$$\text{Drilling Mud: } \rho_1 = 1200\frac{\mathrm{kg}}{\mathrm{m}^3}, n_1 = 1, \kappa_1 = 0.02\ \mathrm{Pa.s}, \tau_{Y,1} = 5\ \mathrm{Pa.s}$$

$$\text{Preflush: } \rho_2 = 1200\frac{\mathrm{kg}}{\mathrm{m}^3}, n_2 = 1, \kappa_2 = 0.02\ \mathrm{Pa.s}, \tau_{Y,2} = 0\ \mathrm{Pa.s}$$

$$\text{Cement Slurry: } \rho_3 = 1700\frac{\mathrm{kg}}{\mathrm{m}^3}, n_3 = 0.6, \kappa_3 = 0.4\ \mathrm{Pa.s}^{0.6}, \tau_{Y,3} = 7\ \mathrm{Pa.s}$$

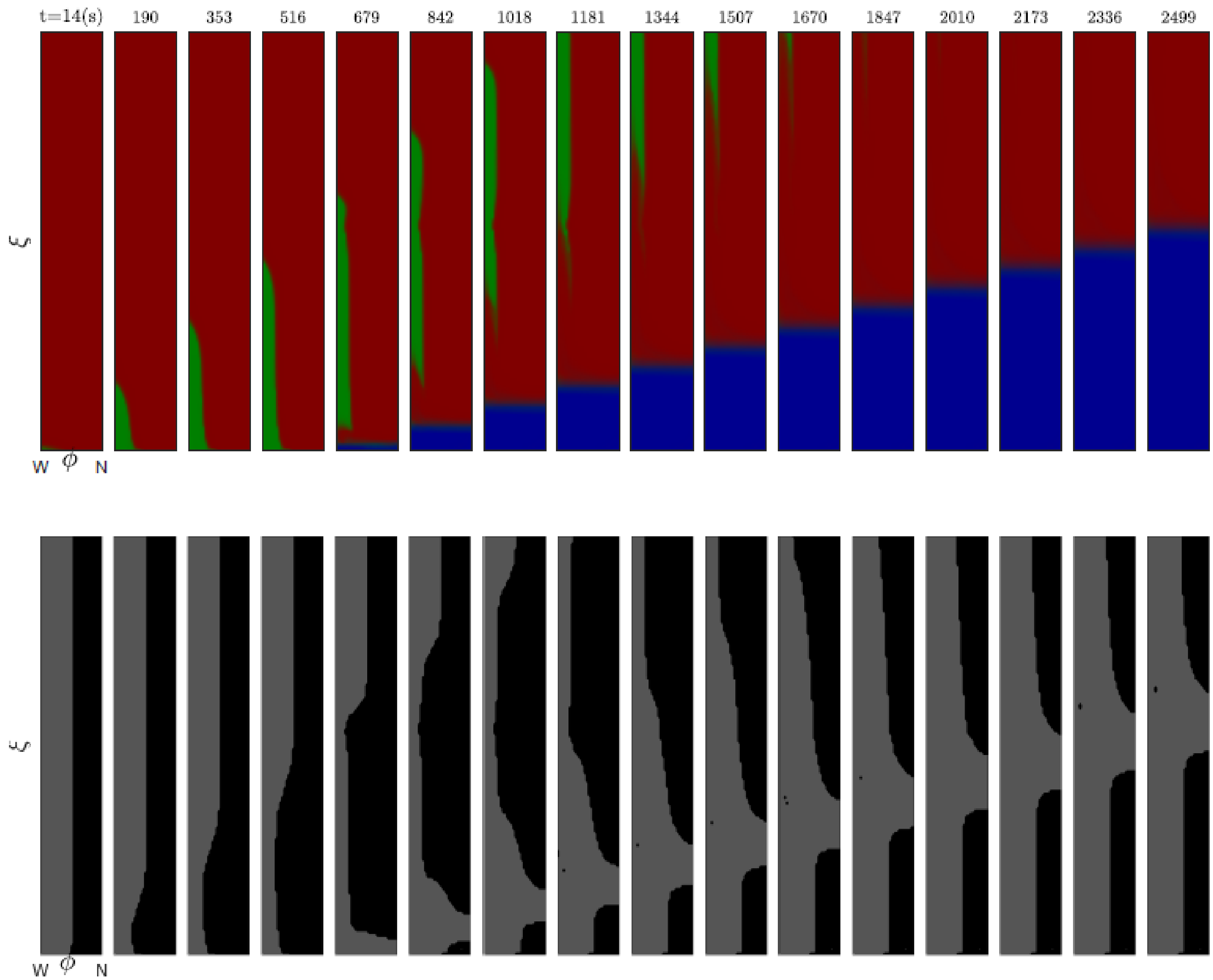

Figure 11: Demonstration of displacement of mud (red) with wash (green) and then cement slurry (blue). Flow regimes are laminar. a) displacement snapshot; b) displacement regime map. Please see the text for the displacement details.

Notice that the mud has fairly typical properties. The preflush is quite different than those commonly used in industry. In particular, it has large viscosity difference and the same density as the mud. The displacement is very unsuccessful, suggesting that for the actual values, the outcome of cementing would be very poor. Figure 11 shows the displacement snapshots when flow rate for both preflush and cement slurry is $Q = 0.015\ \mathrm{m}^3/\mathrm{s}$ and the displacement is laminar. In the top row, the red, green and blue fluids represent mud, preflush and cement slurry, respectively. The bottom row shows the map of displacement regime. Dark gray regions are laminar and black regions are stationary unyielded fluid. The preflush shear viscosity and density are identical to those of mud. However, the mud has a yield stress (of 5 Pa.) and the annulus is slightly eccentric. These combine to favour flow of the preflush along the wide side. We observe that where the preflush flows on the wide side, the wall shear stress generated by the preflush is insufficient to mobilize the mud on the narrow side: a static mud channel is formed. Interestingly, when the cement slurry enters the annulus, both fluids are fully displaced – mainly due to the large density difference..

In the next example, we simulate the very same displacement scenario, except we increase the wash flow rate to $Q = 0.075\ \mathrm{m}^3/s$. This ensures that the wash is flowing in turbulent regime. Figure 12 shows the displacement snapshots together with the regime map. When the wash is pumped, the flow rate is high and therefore, the flow regime is turbulent. However, we still observe a large portion of the mud remains unmobilized until the cement slurry enters. While the displacement is slightly improved compared to the laminar case in Figure 11, it is still far from being a successful displacement. In particular, in the case of both laminar and turbulent flow regimes the mud on the narrow side is not in contact with the wash at all.

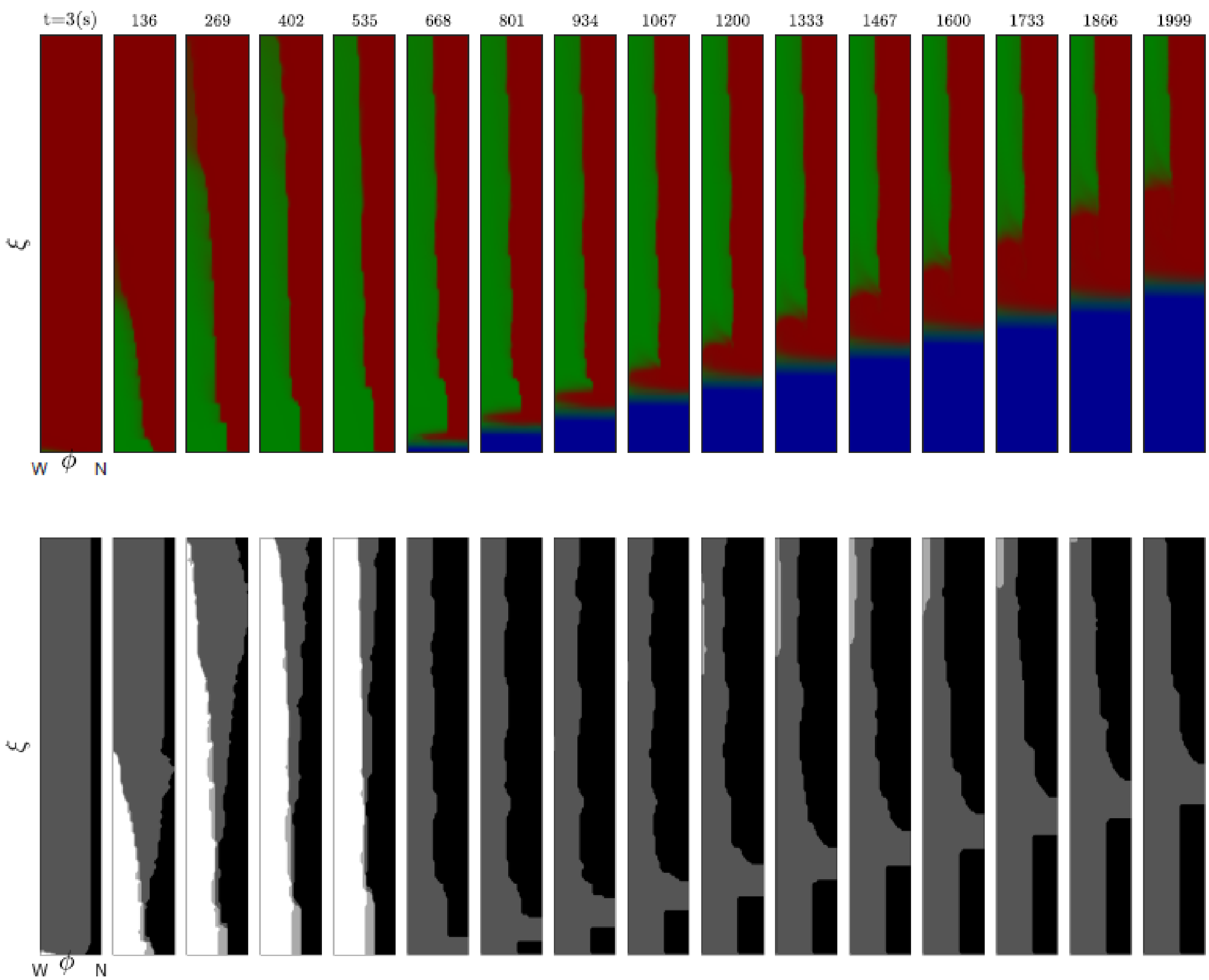

Figure 12: Demonstration of displacement of mud (red) with wash (green) and then cement slurry (blue). Flow regime is turbulent for the wash and laminar for the mud and cement slurry. a) displacement snapshot; b) displacement regime map. Please see the text for the displacement details.

We would like to emphasize that the two examples presented have much better properties than real displacement cases, i.e. where the density difference of the wash is often negative. Thus, one should expect the actual displacement outcome to be much worse than those shown in Figures 11 and 12. Recall that we take the density and viscosity of the wash to be the same as the mud, while in practice, the preflush is much lighter and less viscous than the mud. Furthermore, the annulus is only slightly eccentric. Eccentricity of $e = 0.3$ is perhaps the best we can aim for in many real annuli. In Maleki and Frigaard (2018c) we have conducted more realistic examples, and confirmed that the use of low-viscous lightweight washes is highly ineffective in providing cleaning or displacing the mud.

Finally, we would like to point out that the notion of contact time provides a very inaccurate notion of cleaning. To show this, for any point in the annulus at any time, if the concentration of wash is larger than 20% of the total concentration, we regard that the mud is in contact with the wash. Figure 13 shows the contour of contact time for the examples presented in Figures 11 and 12. We observe that, while the turbulent displacement is comparably better than the laminar, still roughly half of the annulus does not come into contact with the wash. The message here is that contact time is not distributed uniformly around the annulus. In addition, due to the localization observed, increasing wash volumes does not necessarily help with contact time. This largely invalidates the motivation of measuring chemical cleaning efficiency through a bulk contact time. If this concept is to be rescued, it needs local computations, as possible with models such as those used here.

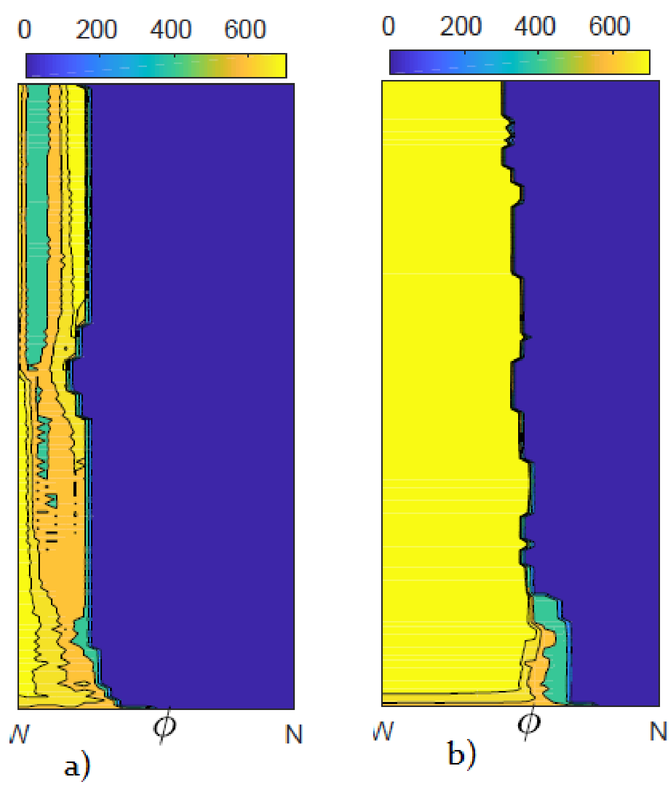

Figure 13: Demonstration of wash contact time (secs) in the annulus. a) Example of Figure 11; b) Example of Figure 12.

Recommendations

The mixed regime annular model has proven very effective in allowing us to both simulate field conditions and to explore the underlying physics behind current practices. We envision that this line of research can be continued in several directions, some of which are currently being pursued under a new project with Schlumberger and NSERC.

1. Benchmarking and validation with experimental measurement.
2. Benchmarking and validation with 3D numerical codes
3. Consequent improvements to the code and model stemming from 1 & 2
4. Extending the Matlab prototype in order to model also the downwards displacement flow in the casing and coupling to the annular flow.
5. Potentially including a model for centralization of the annulus
6. Further work on the foamed cementing model
7. Accelerating the Matlab prototype or switching to another programming language such as C++ to enhance the computational speed.

While we have been active in case-study type approaches to understanding current practices in BC and making recommendations, these efforts are hampered by inadequate data collection for most cementing jobs. Although we will continue with this type of study, we are also interested in other ways of applying this model. One direction that is worth investigating is to simulate a database of successful displacement parameters. This database can then be used for the purpose of machine learning applications: i.e. training a model that can predict if a displacement case is successful or not.

Project 3: A model for foamed cementing

Project 3 concerns the modelling of primary cementing operations that utilize foamed cements. Foamed cements consist of a base cement slurry that suspends a gas phase, typically nitrogen. As a result, they have low density and exhibit higher ductility and higher tensile strength when they hydrate, compared to their conventional counterparts. Some studies show better zonal isolation in foamed cement wells, particularly in wells with high temperature and pressure. This is supposedly because foamed cements are more resilient to cracking caused by temperature and/or pressure-induced stress cycles during production. Furthermore, the expansion of the gas phase during dehydration may compensate the volume loss that typically happens in conventional cements. This lowers the chance of gas migration in foamed cements; (see Hanachi et al (2018) and the reference therein). Despite these apparent advantages, the disastrous Deepwater Horizon oil spill in the Gulf of Mexico has left major concerns in using foamed cements, operationally they are more complex use and risks of poor pressure management are not understood. In practice, some operators favour foamed cements but most do not.

Model Summary

We analyzed foamed cementing using a 1D hydraulics-based model as well as 2D Hele-Shaw cell model similar to that of Project 2. Operationally, the state of a foamed cement is described by a parameter called *quality* q, defined by:

$$q = \frac{\dot{Q}_g}{\dot{Q}_g + \dot{Q}_c},$$

where $\dot{Q}_c$ and $\dot{Q}_g$ are volumetric flow rate of the liquid (cement) and gas phases. Assuming that the gas bubbles are well dispersed in the liquid phase, quality would be equal to volumetric gas fraction (α). Mathematically, it is more convenient to work with mass gas fraction Y_g. Assuming that the gas obeys the ideal gas law, the density of a foamed cement varies with pressure according to the following equation:

$$\rho = \alpha\rho_g + (1-\alpha)\rho_c = \frac{1}{Y_g/\rho_g + (1-Y_g)/\rho_c}, \qquad \rho_g = \frac{pM}{RT}$$

where p and T are gas pressure and temperature, M is the molar mass of the gas and R is the universal gas constant and ρ_g and ρ_c are the gas and cement density, respectively.

Following a 1D approach, in Hanachi et al. (2018) we showed that mass balance simplifies to:

$$\frac{\partial Y_g}{\partial t} + w\frac{\partial Y_g}{\partial z} = 0,$$

For a given pressure, Y_g and then subsequently ρ are computed. Then axial velocity w is then given by

$$w = \frac{\dot{M}}{\rho A} = \frac{\dot{Q}_c \rho_c + \dot{Q}_g \rho_g}{A}\left(\frac{Y_g}{\rho_g} + \frac{1 - Y_g}{\rho_c}\right).$$

Following the hydraulic framework established in Project 1, we can then calculate the wall shear stress τ_w and update pressure at the next spatial cell. This procedure continues until we reach to the bottom of the well. Notice that the rheological parameters of the foamed cement is a weak function of gas fraction (and therefore pressure). See Hanachi et al. (2018) for more details.

As the foamed cement moves upward in the annulus, the gas expands and density of the foam reduces. As a result, Density-driven instabilities might grow in the annulus. Unfortunately, 1D models are inherently incapable of capturing these instabilities. Therefore, better understanding of the effect of compressibility of foamed cement requires a more sophisticated model. In Hanachi et al. (2018), we developed a 2D model, similar to that of Project 2. The main difference of this model compared to that of Project 2 is that since volume of the cement is not constant anymore, we ought to work with the mass streamfunction instead of volumetric streamfunction. More specifically, the streamfunction equation is

$$\boldsymbol{\nabla}_{\mathbf{a}}.\left(\frac{\tau_w(|\nabla_{\mathrm{a}}\Psi_{\mathrm{M}}|)}{H|\nabla_{\mathrm{a}}\Psi_{\mathrm{M}}|}\nabla_{\mathrm{a}}\Psi_{\mathrm{M}} + \mathbf{b}\right) = 0$$

where the mass streamfunction Ψ_M is defined by:

$$(w, -v) = \frac{1}{2\rho H}\nabla_a \Psi_M.$$

Assuming laminar flow regime, the equation for fluid concentration is:

$$\frac{\partial Y_j}{\partial t} + (v, w).\nabla_a Y_j = 0.$$

Here index j refers to all incompressible fluids preceding the foamed cement and the gas phase of the foamed cement.

Density-Driven Instability

In Hanachi et al. (2018), we investigate several of cases of foamed cementing under various input. Here we only discuss one particular example, where density instabilities appear. Consider a $500\ \mathrm{m}$ deep, vertical annulus with inner and outer diameters of $20.3\ \mathrm{cm}$ and $25.4\ \mathrm{cm}$. The annulus is initially filled with a drilling mud which is to be displaced with a nitrogen-foamed cement. The properties of mud and pure cement (liquid phase) are:

$$\rho_1 = 1400\frac{\mathrm{kg}}{\mathrm{m}^3}, n_1 = 1, \kappa_1 = 0.02\ \mathrm{Pa.s}, \tau_{Y,1} = 4\ \mathrm{Pa.s}$$

$$\rho_{\mathrm{c}} = 1800\frac{\mathrm{kg}}{\mathrm{m}^3}, n_{\mathrm{c}} = 1, \kappa_{\mathrm{c}} = 0.04\ \mathrm{Pa.s}, \tau_{Y,\mathrm{c}} = 8\ \mathrm{Pa.s}.$$

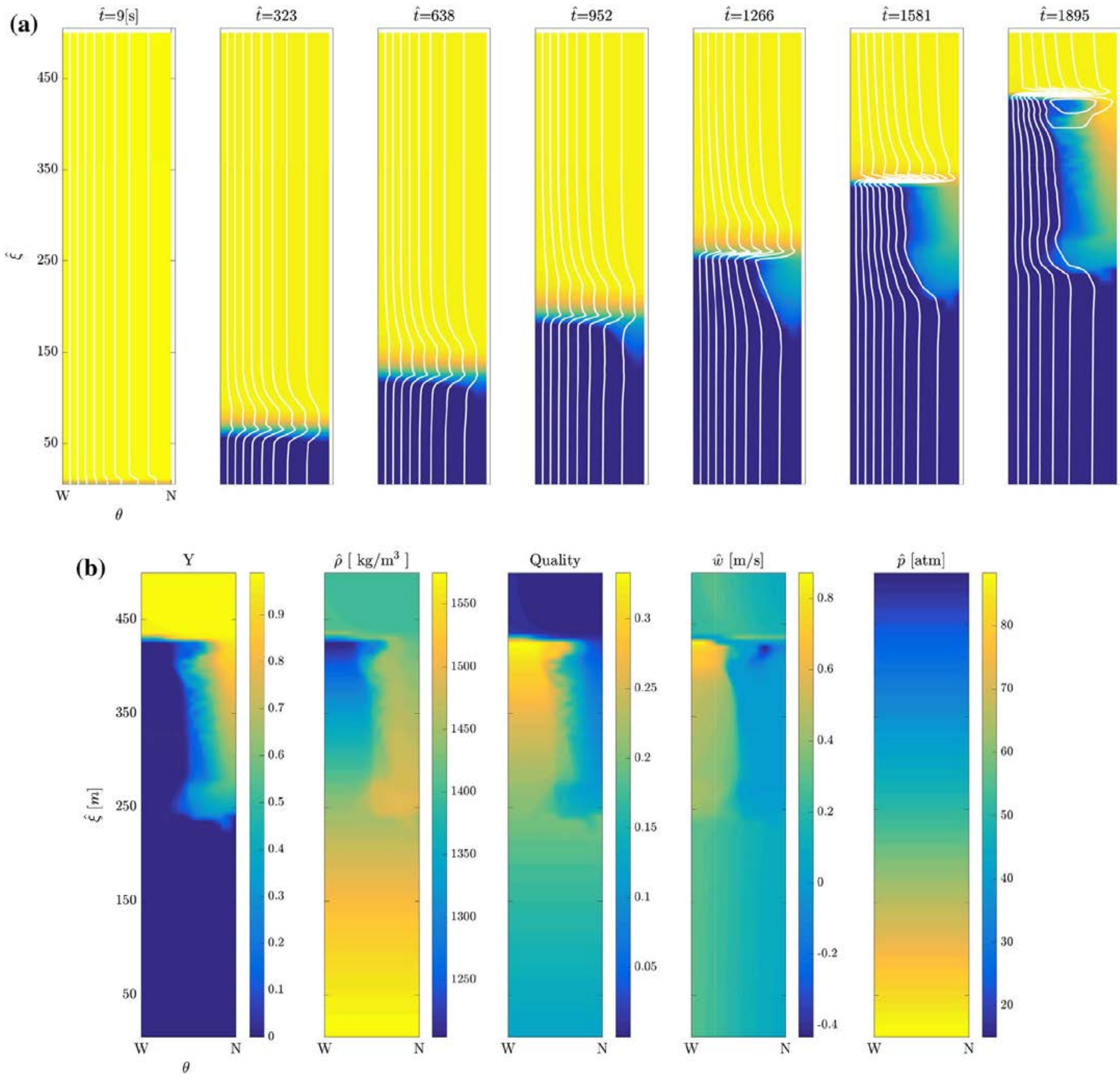

Figure 14: Demonstration of development and growth of density-driven instabilities in primary cementing using foamed cements. Displacement details can be found in the text.

The temperature is fixed at 300 K. The pressure at the surface of casing is 20 atm. The gas and cement flow rates at the top of casing are $\dot{Q}_g = 0.02\ \mathrm{m}^3/s$ and $\dot{Q}_c = 0.03\ \mathrm{m}^3/s$; i.e. inlet quality of 40%. Figure 14a shows the displacement snapshots. The displacement is initially steady, uniformly moving around annulus. Approximately halfway through the annulus, the displacing fluid density is no longer large enough to displacement the mud. Therefore, the displacement begins to become unsteady, rapidly progressing on the wide side of the annulus. What happened here is that as the foamed cement moves up the annulus, the pressure drops, allowing the gas to expand. Consequently, the density of the displacing fluid continuously decreases, and at some point it falls below that of the displaced fluid. The displacing fluid is therefore no longer able to displace the mud on the narrow side, the front begins to elongate and the density difference now across the interface instigates growth of density-driven instabilities, leading to the observed mixing.

Interestingly, additional simulations we have run confirm that the pure cement by itself was perfectly capable of providing a steady displacement of the mud. In other word, had we not used the gas in the cement, the displacement would have been carried out successfully. However, the compressibility of the gas diminishes the ability of the cement to displace.

Summary and Key Results

The results of Project 3 can be summaries by the following remarks:

1. Somewhat surprisingly, the form of the streamfunction equation is near-identical with that for incompressible displacements obtained in Project 2. The main difference is that, due to the compressibility, we use a mass streamfunction Ψ_M instead of the usual volumetric streamfunction.

2. Buoyancy-driven instabilities are triggered at some threshold value of density difference, when the stabilizing viscosity ratio is overcome. More clearly, as the foamed slurry displaces upwards in the annulus the density falls, eventually dropping below that of the drilling mud. At some distance above this, the instability starts.

3. This threshold type of instability is reminiscent of miscible porous media displacement instabilities.

4. The instability is triggered lower in the annulus for a more eccentric annulus, as the density difference is progressively less effective on the narrow side of the annulus. As a result, we observe a significant residual mud layer emerges on the narrow side of the annulus. The root cause of the instability is the decreasing density of the foamed slurry.

The key message of Project 3 is that the occurrence of this type of flow instability raises serious questions about the usage of foamed cements. A key motivation for using foamed cements is control of the hydrostatic gradient in the annulus, i.e. low density. If it is necessary to keep the slurry density above the mud density to avoid instabilities, this limits the range of density reduction. More specifically, foamed cement appears problematic from the point of view of hydrodynamic instability. The density-driven instabilities are amplified as the foam expands along the annulus, which self-reinforces the destabilizing mechanism. Although here we have used a cement slurry that is more viscous than the mud, this is not always the case and the uncertainty of foamed cement rheology with pressure (and temperature) means that a viscosity gradient threshold might not be reliable. Even if the foamed cementing operation is undertaken under a controlled pressure, loss of control in this way presents dangers.

Project 4: Interface tracking in primary cementing

Project 4 was conducted in collaboration with SINTEF industries as part of the FLUCCS project of the Norwegian Research Council (project 268510). The goal of this project is to enhance the quality of cementing measurements. Currently, quality of cementing is most commonly measured using a cement bond log (CBL). CBL measures acoustic amplitude, travel time and attenuation. The acoustic signals are processed to infer information about the bonding of cement-casing and cement-formation pairs. CBL reading are reliable in evaluating the top of cement, as well as identifying the large defects. However, small-scale features such as a mud layer may not be detected in CBL readings. In addition, CBL readings involve a costly time delay, thus in many cases, CBL is not run. Furthermore, CBL can only be run when the cement is set, and therefore no corrective measures can be pursued immediately, had the cementing gone obviously wrong. The objective of Project 4 is to design a new methodology to measure cement quality that addresses the above issues. In particular, if the measurement technology can be run during (or shortly after) cementing, necessary corrective procedures (if any) can be followed.

Analysis

The main idea of this proposed methodology is to track the displacement interface in real-time. To track the interface, one of fluids is seeded with particles with a density intermediate between displaced and displacing fluids density, (here we assume the displacing fluid is heavier than the displaced fluid). Because of the buoyancy force, the particles tend to move toward the interface. Since the direction the of buoyancy force experienced by the particle changes across the interface, if the particles reach the interface, they remain trapped at the interface. Tracking the interface then amounts to tracking the particles. The latter is an acknowledged challenge, but not the focus here.

For the particles to reach to the interface, the buoyancy force on the particle has to be sufficiently large. The reason is that in an eccentric vertical well, the velocity of the displacement front can be quite different from velocity far from the interface. As was discussed at length in Project 3, far from the interface, the flow is faster on the wide side and slower on the narrow side. In the vicinity of the interface however, the buoyancy forces compete against this azimuthal bias in velocity field. This difference of the interface and the far-field velocity plays a key role in the success or failure of the methodology described above.

This analyze this more carefully, in Maleki and Frigaard (2018a), we designed a 1D toy model, as well as a 2D model. In the one-dimensional model, the particle momentum velocity is given by:

$$m_p \frac{\mathrm{d}^2 z_p}{\mathrm{d}t^2} = F_D + F_B$$

where z_p is the particle axial position, m_p is the particle mass, and F_D and F_B are the drag force and buoyancy force exerted on the particle. The buoyancy force and the drag force can be approximated as follows:

$$F_B = \frac{\pi}{6}(\rho_f - \rho_p) g \, d_p^3 \text{ and } F_D = -3\pi\mu_f d_p \left(\frac{\mathrm{d}\, z_p}{\mathrm{d}t} - w_f\right).$$

Here d_p and ρ_p are particle diameter and density, w_f in the fluid velocity and μ_f is the (effective) viscosity of the carrier fluid. In Maleki and Frigaard (2018a), we carried out a scaling analysis for the momentum equation and identify a critical dimensionless parameter Bu, defined by:

$$Bu = \frac{\Delta\rho_f g d_p^2}{w_i \mu}.$$

Bu is the buoyancy number representing the ratio of buoyancy force and viscous drag that the particles experience. If the particle density is the average of the two fluids densities, the 1D analysis leads to the following criterion that guarantees the particles reach the interface:

$$Bu \geq 18.$$

Interestingly, what is missing in the 1D analysis is the secondary flows that are generated near the interface due to density or viscosity difference. These secondary flows move the displacing fluid from the wide side to the narrow side (and vice versa for the displaced fluid). Therefore, one can expect particles to move substantially in the azimuthal direction when they are close to the interface. To analyze this more carefully, we also performed 2D analysis. Briefly speaking, this methodology consists of two stages: We first compute a 2D gap-averaged velocity field using the model of Project 2 and then use the fluid velocity field in the particle momentum equations. In addition to the axial momentum equation, we also need to consider azimuthal momentum:

$$m_p \frac{\mathrm{d}^2 \phi_p}{\mathrm{d}t^2} = F_D = -3\pi\mu_f d_p \left(\frac{\mathrm{d}\phi_p}{\mathrm{d}t} - \frac{v_f}{\frac{\pi}{2}(r_i + r_o)}\right),$$

where r_i and r_o are the inner and outer radius of the annulus. Notice that the well is assumed vertical, so buoyancy force does not have any azimuthal component. Upon integrating the axial and azimuthal momentum equations, the position of the particles is computed as a function of time. It is worth mentioning that this process is based on the assumption that the particles are small enough that their contribution to the fluid momentum is insignificant; i.e. the coupling is only one-directional.

Examples

Here we illustrate the dynamic of particle motion in the context of an example. Consider a vertical annulus with inner and outer radius of $r_i = 22.75$ cm and $r_o = 25.25$ cm and eccentricity $e = 0.2$. We only simulate the bottom 50 m of the annulus. The properties of the displaced and displacing fluids are fixed at

$$\rho_1 = 1500 \frac{\mathrm{kg}}{\mathrm{m}^3}, n_1 = 1, \kappa_1 = 0.05 \text{ Pa.s}, \tau_{Y,1} = 0 \text{ Pa.s} \rho_2 = 1700 \frac{\mathrm{kg}}{\mathrm{m}^3}, n_2 = 1, \kappa_2 = 0.01 \text{ Pa.s}, \tau_{Y,2} = 0 \text{ Pa.s}.$$

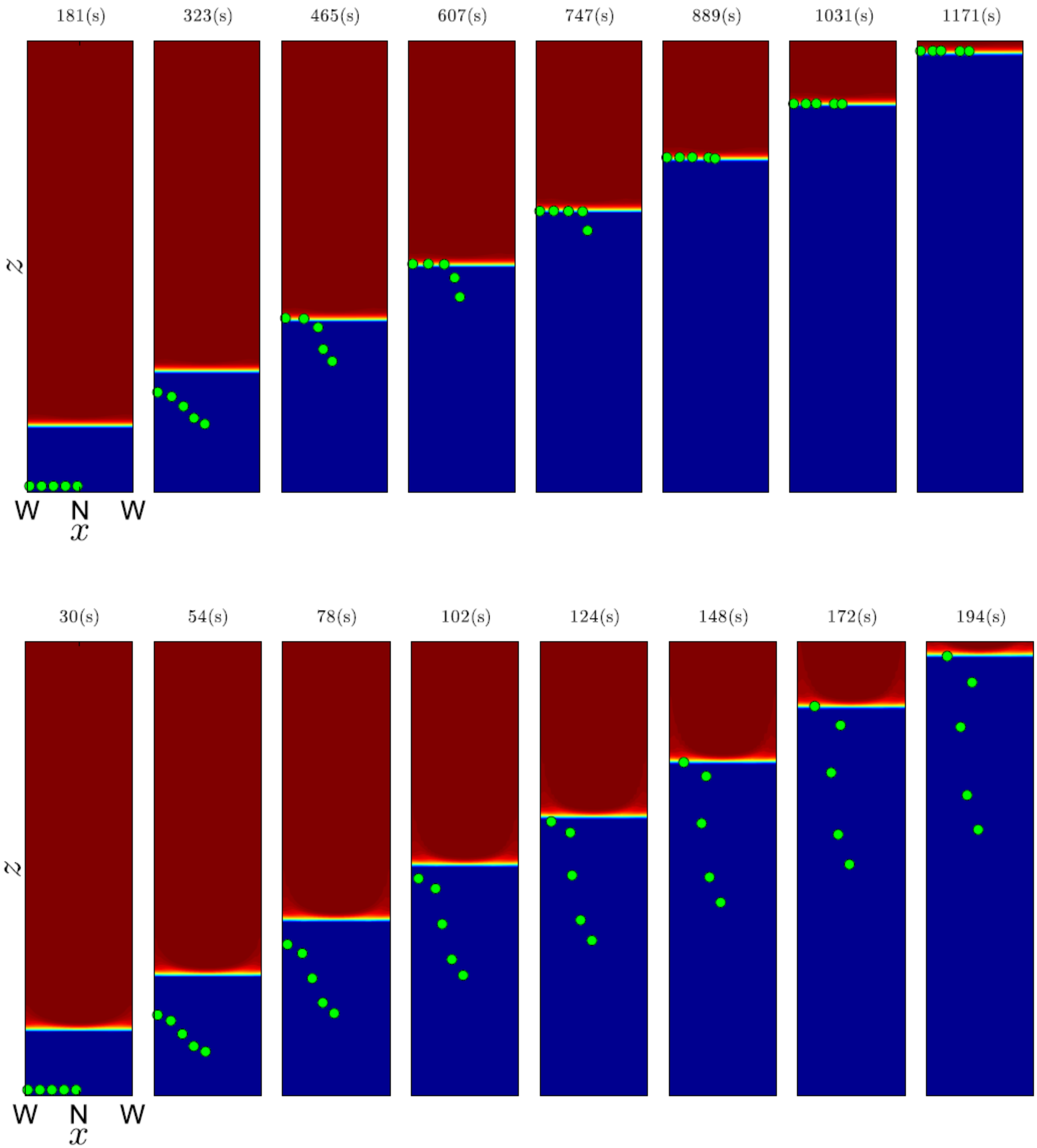

Figure 15:Demonstration of interface tracking using particles with intermediate density. Top row (Bu =30) successful tracking of the interface. Bottom Row (Bu = 7.5) interface tracking fails.

Similar to previous examples, the annulus is initially filled with the displaced fluid and displacing fluid enters the annulus at a prescribed rate. We consider two flow rates as $Q = 0.001\ \mathrm{m^3/s}$ (Figure 15 a) and $Q = 0.004\ \mathrm{m^3/s}$ (Figure 15 b). For both cases, when the displacement interface is at height $z = 4\ \mathrm{m}$, we release 5 particles with density of $\rho_p = 1600\ \mathrm{kg/m^3}$ and diameter $d_p = 2\ \mathrm{mm}$. The particles are equally distributed around half of the annulus. The displacement snapshots together with the position of particles is shown in Figure 15. Notice that here we have shown the full annulus. Clearly, the displacement is perfectly steady, thanks to the density difference of displaced and the displacing fluids. In Figure 15a, the particles successfully reach to the interface after a few minutes, whereas in Figure 15b, most of the particles do not reach to the interface and instead they reach a secondary equilibrium state with a velocity smaller than that of interface. Therefore, their distance from the interface continually increase. Figure 15a represents a case where the interface is successfully tagged. The combination of fluid and parameters in this case lead to $Bu = 30$, which is conveniently above the critical value $Bu = 18$. On the contrary, Figure 15b demonstrates a case where the interface tracking fails. The Buoyancy number associated with this case is $Bu = 7.5$, which is below the critical value.

In Maleki and Frigaard (2018a), we have analyzed several other examples including with shear-thinning and yield stress fluids. An experimental part of the project and CFD computations are being carried out by our collaborators.

Key results and summary

In project 4, we conducted a feasibility study for a novel technique to track the interface between two fluids in annular displacement flows. Our technique is based on exploiting the density difference between successive fluids pumped in order to design a tracer particle to sit at the interface. Tracking the particles sitting at the interface allows us to track the displacement flow interface, which in turn provides a more accurate assessment of the cement job. We showed that for the particles to reach to the interface, the following heuristic criteria may be sufficient, provided that the well is not too eccentric:

$$Bu \geq 18$$

For a range of parameters relevant to laminar primary cementing, the criterion above is marginally satisfied. In order to widen this margin, two ideas are explored (i) We can adjust the particle density which we have fixed to the mean density of the 2 fluids, and (ii) start the particles closer to the interface. The former of these acts to increase buoyancy force exerted on the particle when in the displacing fluid, with the risk of losing stability in the displaced fluid, should the particles be disturbed from the interface. Releasing the particle nearer to the interface will reduce the differential velocity $w - w_i$. Operationally, transporting tracer particles within the bottom plug (or any preceding plug) offers an easy way to deliver the particles downhole and into the flow when the plug bursts.

Application and Dissemination of Results

Over the course of the project (and preceding projects), we have disseminated results in the following places, as well as in the PhD thesis of Dr. Amir Maleki (http://hdl.handle.net/2429/67903) and master thesis of Ms. Nikoo Hanachi (http://hdl.handle.net/2429/65133).

JOURNAL PAPERS:

- Maleki and I.A. Frigaard. "Axial dispersion in weakly turbulent flows of yield stress fluids" J. non-Newt. Fluid Mech., 235,1–19, 2016.
- Maleki and I.A. Frigaard. "Primary cementing of oil & gas wells in turbulent and mixed regimes". J. Eng. Math., 107, 201–230, 2017
- Maleki and I.A. Frigaard. "Tracking fluid interfaces in primary cementing of surface casing" Phys. Fluids, 30, 093104, 2018a
- Maleki and I.A. Frigaard. "Turbulent displacement flows in primary cementing of oil and gas wells" Phys. Fluids, 30, 123101, 2018b
- N. Hanachi, A. Maleki, and I.A. Frigaard. "A model for foamed cementing of oil and gas wells" J. Eng. Math., 113, 93-121, 2018.
- Renteria, A. Maleki, I.A. Frigaard, B. Lund, A. Taghipour, J. and Ytrehus, "Effects of irregularity on displacement flows in primary cementing of highly deviated wells" J. Petr. Sci. Eng, 172, 662–680, 2019
- Maleki and I.A. Frigaard. "Comparing laminar and turbulent primary cementing flows" J. Petrol. Sci. Eng., (under review)

CONFERENCES:

- Maleki and I.A. Frigaard, "Real-time measurement of eccentricity in primary cementing of oil and gas wells" International Conference on Ocean, Offshore & Arctic Engineering, Scotland, 2019
- Maleki and I.A. Frigaard, "Interface tracking in primary cementing of oil and gas wells" International conference on multiphase flows, Brazil, 2019

- Renteria, A. Maleki, I.A. Frigaard, B. Lund, A. Taghipour, J. and Ytrehus, “Displacement efficiency for primary cementing of washout sections in highly deviated wells" SPE Asia Pacific Oil and Gas Conference and Exhibition, Australia, 2018

- Renteria, A. Maleki, I.A. Frigaard, “Rheological and geometric effects in cementing irregularly shaped wells" Nordic Rheology Conference, Norway, 2018

- Maleki and I.A. Frigaard “Using lightweight or low viscosity preflushes for primary cementing of surface casing" International Conference on Ocean, Offshore & Arctic Engineering, Spain, 2018

- Maleki and I.A. Frigaard “Interface tracking in primary cementing of oil and gas wells" International Conference on Ocean, Offshore & Arctic Engineering, Spain, 2018

- N. Hanachi, A. Maleki and I.A. Frigaard “Displacement of foamed cement in primary cementing”, Annual European Rheology Conference, Italy, 2018

- Maleki, I.A. Frigaard “Axial dispersion in weakly turbulent flows of yield stress fluid” Poster presented at the Unconventional Gas Technical Forum, Canada, 2016

- Maleki, I.A. Frigaard “Annular Cement Displacement in Weakly Turbulent Regime” Poster and proceedings paper at the 17th International Congress on Rheology (ICR), 2016, Japan.

- Maleki, I.A. Frigaard “Axial dispersion in weakly turbulent flows of yield stress fluids” Poster and proceedings paper at the 24th International Congress on Theoretical and Applied Mechanics (ICTAM), 2016, Canada.

- Maleki, I.A. Frigaard “Annular turbulent cement displacement during primary cementing” Poster presented at the Unconventional Gas Technical Forum, Canada 2015

References

E. Atherton, D. Risk, C. Fougère, M. Lavoie, A. Marshall, J. Werring, J.P. Williams, and C. Minions, "Mobile measurement of methane emissions from natural gas developments in Northeastern British Columbia, Canada" Atmos. Chem. Phys. 17, 12405-12420, 2017.

S.H. Bittleston, J. Ferguson, and I.A. Frigaard, Mud removal and cement placement during primary cementing of an oil well- Laminar non-Newtonian displacements in an eccentric annular Hele-Shaw cell" J. Eng. Math., 43, 229–253, 2002.

D.W. Dodge and A.B. Metzner, "Turbulent flow of non-Newtonian systems" AIChE J., 5, 189–204, 1959

D. Dusterhoft, G. Wilson, and K. Newman, "Field Study on the use of cement pulsation to control gas migration", SPE paper 75689-MS, 2002

M.B. Dusseault, R.E. Jackson, and D. MacDonald, "Towards a Road Map for Mitigating the Rates and Occurrences of Long-Term Wellbore Leakage." Consulting report from Univ. Waterloo and Geofirma Engng. May 22, 2014.

S. Enayatpour and E. van Oort. Advanced modeling of cement displacement complexities. In SPE/IADC Drilling conference and Exhibition, SPE paper 184702, 2017.

L. Gorokhova, A.J. Parry, and N.C. Flamant. "Comparing soft-string and stiff-string methods used to compute casing centralization" SPE Drill. Completion, 29, 106-114, 2014.

D.J. Guillot, B. Froelich, E. Caceres, and R. Verbakel. "Are casing centralization calculations really conservative?" IADC/SPE Drilling Conference, SPE paper 112725, 2008.

N. Hanachi, A. Maleki, and I.A. Frigaard. "A model for foamed cementing of oil and gas wells" J. Eng. Math., 113, 93-121, 2018.

F.C. Kettl, M.G. Edwards, and R.L. Covington. Practical horizontal cementing today. In Middle East Oil Show, SPE paper 25546, 1993.

P.R. Khalilova, B.E. Koons, D.W. Lawrence, and A. Elhancha. Newtonian fluid in cementing operations in deepwater wells: Friend or foe? In SPE Annual Technical Conference and Exhibition, SPE paper number 166456, 2013.

A. Lavrov and M. Torsater. Physics and Mechanics of Primary Well Cementing. Springer, 2016.

A. Maleki and I.A. Frigaard. "Axial dispersion in weakly turbulent flows of yield stress fluids" J. non-Newt. Fluid Mech., 235,1–19, 2016.

A. Maleki and I.A. Frigaard. "Primary cementing of oil & gas wells in turbulent and mixed regimes". J. Eng. Math., 107, 201–230, 2017

A. Maleki and I.A. Frigaard. "Tracking fluid interfaces in primary cementing of surface casing" Phys. Fluids, 30, 093104, 2018a

A. Maleki and I.A. Frigaard. “Turbulent displacement flows in primary cementing of oil and gas wells” Phys. Fluids, 30, 123101, 2018b

A. Maleki and I.A. Frigaard. “Using lightweight or low viscosity preflushes for primary cementing of surface casing” 37th International Conference on Ocean, Offshore & Arctic Engineering, 2018c

A. Maleki and I.A. Frigaard. “Comparing laminar and turbulent primary cementing flows” J. Petrol. Sci. Eng, (submitted), 2019

A. Maleki, “Annular displacement flows in turbulent and mixed flow regimes” PhD Dissertation, University of British Columbia, 2019

A.B. Metzner and J.C. Reed, “Flow of non-Newtonian fluids: Correlation of the laminar, transition, and turbulent-flow regions” AIChE J., 1, 434–440, 1955

E.B. Nelson. Well cementing. Newnes, 1990.

E.B. Nelson and D. Guillot. Well cementing. Schlumberger, 2006.

Renteria, A. Maleki, I.A. Frigaard, B. Lund, A. Taghipour, J. and Ytrehus, “Effects of irregularity on displacement flows in primary cementing of highly deviated wells” J. Petr. Sci. Eng, 172, 662–680, 2019

C.W. Sauer. Mud displacement during cementing: state of the art. J. Petrol. Tech., 39, 1091-1101, 1987.

G.I. Taylor “The dispersion of matter in turbulent flow through a pipe” Proceedings of Royal Society A, 223, 446–468, 1954